NANOSTRUCTURED ADSORBENTS

Ralph T. Yang

Department of Chemical Engineering, University of Michigan
Ann Arbor, Michigan 48109

ADVANCES IN CHEMICAL ENGINEERING, VOL. 27 0065-2377/01 $35.00

08/18/2001 04:12 PM Chemical Engineering-v27 PS068-03.tex PS068-03.xml APserialsv2(2000/12/19) Textures 2.0

This chapter discusses the fundamental principles for designing nanoporous adsorbents and recent progress in new sorbent materials. For sorbent design, detail discussion is given on both fundamental interaction forces and the effects of pore size and geometry on adsorption. A summary discussion is made on recent progress on the following types of materials as sorbents: activated carbon, activated alumina, silica gel, MCM-41, zeolites, π-complexation sorbents, carbon nanotubes, heteropoly compounds, and pillared clays.

I. Introduction

Since the development of synthetic zeolites and pressure swing adsorption (PSA) cycles, adsorption has been playing an increasingly important role in gas separation and purification in chemical and petrochemical industries (Yang, 1997). Even though new applications for gas separations by adsorption are continually being developed, the most important applications have been air separation (for production of O_2 and N_2) and hydrogen separation (from fuel gases). Approximately 20% of the O_2 and N_2 are currently being produced by PSA, and the share is continuing to increase. Drying by PSA is already a mature technology. Other applications, including environmental control, are on the horizon.

The increasing industrial applications for adsorption have stimulated a growing interest in research. The research has been advancing on several fronts: thermodynamics of adsorption (particularly statistical mechanics), diffusion of pores, PSA simulation, new process and cycle development, sorbent characterization, and development of new sorbents. Significant advances have been made on all fronts during the last decade.

Applications for adsorption have been limited by the availability of sorbents. The economics of all adsorption processes are also limited by the sorbent; improvement in the sorbent will lead to improved economics. Hence, major advances in gas adsorption technology will come from the development of new sorbents. For this reason, special attention will be given to new sorbent development during the last decade.

The adsorptive separation is achieved by one of the three mechanisms: steric, kinetic, or equilibrium effect. The steric effect derives from the molecular sieving property of zeolites. In this case only small and properly shaped molecules can diffuse into the adsorbent, whereas other molecules are totally excluded. Kinetic separation is achieved by virtue of the differences in diffusion rates of different molecules. A large majority of processes operate through the equilibrium adsorption of mixture and hence are called *equilibrium separation processes.*

There are only four types of sorbents that have dominated the commercial use of adsorption: activated carbon, molecular-sieve zeolites, silica gel, and activated alumina. Estimates of worldwide annual sales of these sorbents are as follows (Humphry and Keller, 1997):

activated carbon	\$1 billion;
molecular-sieve zeolites	\$100 million;
silica gel	\$27 million;
activated alumina	\$26 million.

Among these sorbents, only activated carbon is *hydrophobic*. However, water vapor also adsorbs, and it does decrease the sorbent capacity for hydrocarbons quite substantially (Doong and Yang, 1987; Huggahalli and Fair, 1996; Russel and LeVan, 1997).

The availability of new sorbents is limiting the application of adsorption for new applications in separation and purification processes.

II. Fundamental Factors for Designing Adsorbents

Selection or synthesis of adsorbents for a given target adsorbate molecule is based on the adsorption isotherm. With the availability of high-speed computing, it is now possible to calculate the adsorption isotherms based on: (1) interaction potentials and (2) structure or geometry of the adsorbent. Hence we begin with a review of the basic forces between the adsorbent and adsorbate, paying particular attention to adsorbent design.

A. Potential Energies for Adsorption

Adsorption occurs when the interaction potential energy ϕ is equal to the work done to bring a gas molecule to the adsorbed state. As a first approximation, the adsorbed state is assumed to be at the saturated vapor pressure.

$$-\phi = -\Delta G = \int_P^{P_0} V\, dP = RT \ln \frac{P_0}{P}, \tag{1}$$

where ΔG is the free energy change and P_0 is the saturated vapor pressure. Hence P is the pressure when adsorption occurs for the given ϕ. (So ϕ is actually the sorbate–sorbate interaction energy on the liquid surface.)

The total potential between the adsorbate molecules and the adsorbent is the sum of the total adsorbate–adsorbate and the adsorbate–adsorbent potentials:

$$\phi_{\text{total}} = \phi_{\text{adsorbate-adsorbate}} + \phi_{\text{adsorbate-adsorbent}} \tag{2}$$

The adsorbent has only a secondary effect on the adsorbate–adsorbate interaction. For this reason, we will focus our attention on the second term, adsorbate–adsorbent potential, and refer to this term as ϕ.

There are three basic types of contributions to the adsorbate–adsorbent interactions: dispersion, electrostatic, and chemical bond. The latter, chemical bond, has been explored for adsorption only recently. Weak chemical bonds, particularly the broad type of bonds involving π electrons, or π-complexation, offer promising possibilities for designing new and highly selective sorbents. The subject of π-complexation sorbents will be discussed in a separate section. For physical adsorption, the adsorbate–adsorbent potential is

$$\phi = \phi_D + \phi_R + \phi_{\text{Ind}} + \phi_{F\mu} + \phi_{\dot{F}Q}, \tag{3}$$

where ϕ_D = dispersion energy, ϕ_R = close-range repulsion energy, ϕ_{Ind} = induction energy (interaction between an electric field and an induced dipole), $\phi_{F\mu}$ = interaction between an electric field (F) and a permanent dipole (μ), and $\phi_{\dot{F}Q}$ = interaction between the field gradient and a quadrupole (Q).

The first two contributions ($\phi_D + \phi_R$) are *nonspecific* (Barrer, 1978), which are operative in all sorbate–sorbent systems. The last three contributions arise from charges (which create electric fields) on the solid surface. (This is a simplified view, because an adsorbate molecule with a permanent dipole can also induce a dipole in the sorbent if the sorbent is a conductor (Masel, 1996)). For activated carbon, the nonspecific interactions dominate. For metal oxides and ionic solids, the electrostatic interactions often dominate, depending on the adsorbate. For adsorbate with a quadrupole, the net interaction between a uniform field and the quadrupole is zero. However, the quadrupole interacts strongly with the field gradient, hence the term $\phi_{\dot{F}Q}$.

The individual contributions to the total potential have been reviewed and discussed in detail in the literature (Barrer, 1978; Masel, 1996; Razmus and Hall, 1991; Gregg and Sing, 1982; Steele, 1974; Adamson, 1976; Rigby *et al.,* 1986; Israelachilli, 1992; Young and Crowell, 1962; Ruthven, 1984; Ross and Olivier, 1964). Their functional forms are summarized here. All interactions are given between an atom (or a charge) on the surface and the adsorbate molecule.

Dispersion:

$$\phi_D = -\frac{A}{r^6}. \tag{4}$$

Repulsion:

$$\phi_R = +\frac{B}{r^{12}}. \tag{5}$$

Field (of an ion) and induced-point dipole:

$$\phi_{\text{Ind}} = -\frac{1}{2}\alpha F^2 = -\frac{\alpha q^2}{2r^4(4\pi\in_0)^2}. \tag{6}$$

Field (of an ion) and point dipole:

$$\phi_{F\mu} = -F\mu\cos\theta = -\frac{q\mu\cos\theta}{r^2(4\pi\epsilon_0)}. \tag{7}$$

Field gradient ($\dot{F}$) and linear point quadrupole:

$$\phi_{\dot{F}Q} = \frac{1}{2}Q\dot{F} = -\frac{Qq(3\cos^2\theta - 1)}{4r^3(4\pi\epsilon_0)}, \tag{8}$$

where A and B are constants, α = polarizability, F = electric field, q = electronic charge of the ion on the surface, $\in_0$ = permittivity of a vacuum, μ = permanent dipole moment, θ = angle between the direction of the field or field gradient and the axis of the dipole or linear quadrupole, and Q = linear quadrupole moment (+ or –). The important parameter, *r,* is the distance between the centers of the interacting pair.

The dispersion and repulsion interactions form the Lennard–Jones (Barrer, 1978; Masel, 1996; Razmus and Hall, 1991; Gregg and Sing, 1982; Steele, 1974; Adamson, 1976; Rigby *et al.,* 1986) potential, with an equilibrium distance (r_0) where $\phi_D + \phi_R = 0$. This distance is taken as the mean of the van der Waals radii of the interacting pair. Once the attractive, dispersion constant, A, is known, B is readily obtained by setting at $d\phi/dr = 0$ at r_0. Hence, $B = Ar_0^6/2$. The most commonly used expression for calculating A is the Kirkwood–Muller formula:

$$A = \frac{6mc^2\alpha_i\alpha_j}{(\alpha_i/\chi_i) + (\alpha_j/\chi_j)}, \tag{9}$$

where m is the mass of an electron, c is the speed of light, χ is the magnetic susceptibility, and i and j refer to the two interacting atoms or molecules. For $\phi_{F\mu}$ and $\phi_{\dot{F}Q}$, the maximum potentials are obtained when the dipole or quadrupole are arranged linearly with the charge on the surface.

B. Heat of Adsorption

In the last section, we summarized the different contributions to the potential energy for the interactions between an adsorbate molecule (or atom) and an atom on the solid surface. To calculate the interaction energy between the adsorbate molecule and all atoms on the surface, pairwise additivity is generally assumed. The task is then to sum the interactions, pairwise, with all atoms on the surface, by integration.

It can be shown (Barrer, 1978; Ross and Olivier, 1964) that the isosteric heat of adsorption (ΔH) at low coverage is related to the sorbate–sorbent interaction potential (ϕ) by

$$\Delta H = \phi - RT + F(T), \tag{10}$$

where $F(T)$ arises due to the vibrational and translational energies of the adsorbate molecule, and for monatomic classical oscillators, $F(T) = 3RT/2$ (Barrer, 1978). For ambient temperature, $\Delta H \approx \phi$.

C. Effects of Adsorbate Properties on Adsorption: Polarizability (α), Dipole Moment (μ), and Quadrupole Moment (Q)

For a given sorbent, the sorbate–sorbent interaction potential depends on the properties of the sorbate. Among the five different types of interactions, the nonspecific interactions, ϕ_D and ϕ_R, are nonelectrostatic. The most important property that determines these interactions (and also ϕ_{Ind}) is the polarizability, α. On a surface without charges such as graphite, $\phi_{\text{Ind}} = 0$. The value of α increases with the molecular weight, because more electrons are available for polarization. From the expressions for ϕ_D, ϕ_R, and ϕ_{Ind}, it is seen that these energies are nearly proportional to α. The dispersion energy also increases with the magnetic susceptibility, χ, but not as strongly as α.

Table I gives a summary of interaction energies for a number of sorbate–sorbent pairs. Here groupings are made for the theoretical nonelectrostatic ($\phi_D + \phi_R + \phi_{\text{Ind}}$) and the electrostatic ($\phi_{F\mu} + \phi_{\hat{F}Q}$) energies.

The nonelectrostatic energies depend directly on the polarizability of the sorbate molecule. χ makes a contribution to the dispersion energy, and χ also increases with molecular weight.

Two types of sorbents are included in Table I, one without electric charges on the surface (graphitized carbon) and one with charges (zeolites). On carbon, dispersion energy dominates. On zeolites, the permanent dipole and quadrupole can make significant contributions—and, indeed, can dominate—the total energy. N_2 has a strong quadrupole but no permanent dipole; hence, $\phi_{F\mu} = 0$. From Table I shows that $\Phi_{\hat{F}Q}$ accounts for about one-third of the energies on chabazite and Na/mordenite. Na/X zeolite contains more Na^+ ions because its Si/Al ratio is lower than the other two zeolites. Consequently $\phi_{\hat{F}Q}$ contributes about one-half of the interaction energies for N_2 on Na/X. The other sorbate molecules included in Table I have both strong dipoles and quadrupoles (except H_2O, which has a strong dipole only). For adsorption of these molecules on zeolites, the ($\phi_{F\mu} + \phi_{\hat{F}Q}$) interactions clearly dominate.

A comparison of N_2 and O_2 is of particular interest for the application of air separation. Both molecules are nonpolar and have very similar

TABLE I
CONTRIBUTIONS (THEORETICAL) TO INITIAL (NEAR ZERO LOADING) HEAT OF ADSORPTION (EXPERIMENTAL, $-\Delta H$, kcal/mol) (BARRER, 1978; ROSS AND OLIVIER, 1964)

Sorbent	Sorbate[a]	$\alpha \times 10^{24}$ cm^3/molecule	$-\Delta H$	$-(\phi_D + \phi_R + \phi_{\text{Ind}})^b$	$-(\phi_{F\mu} + \phi_{\dot{F}Q})$
Graphitized Carbon	Ne	0.396	0.74	0.73	0
	Ar	1.63	2.12	1.84	0
	Kr	2.48	2.8	2.48	0
	Xe	4.04	3.7	3.1	0
Chabazite	N_2	1.74	8.98	6.45	2.55
	N_2O	3.03	15.3	9.07	6.18
	NH_3	2.2	31.5	7.5	23.8
Na/Mordenite	N_2	1.74	7.0	4.5	2.50
	CO_2	2.91	15.7	6.73	8.93
Na/X	N_2	1.74	6.5	3.10	3.4
	CO_2	2.91	12.2	4.20	7.98
	NH_3	2.2	17.9	3.75	14.2
	H_2O	1.45	≈33.9	2.65	≈31.3

[a]Permanent dipole moments (μ, debye): $N_2O = 0.161$, $NH_3 = 1.47$, $H_2O = 1.84$, all others = 0. Quadrupole moments (Q, erg$^{1/2}$ cm$^{5/2}$ $\times$ 10^{26}): $N_2 = -1.5$, $N_2O = -3.0$, $NH_3 = -1.0$, $CO_2 = -4.3$, all others ≈ 0.

[b]For graphitized carbon, $\phi_{\text{Ind}} = 0$.

polarizabilities and magnetic susceptibilities. However, their quadrupole moments differ by nearly a factor of four ($Q = -0.4$ esu for O_2 and –1.5 esu for N_2). As a result, the adsorption isotherms of N_2 and O_2 on carbon are similar, whereas the isotherm of N_2 is much higher than that of O_2 on zeolites. The contribution of interaction between the field gradient and the quadrupole moment of N_2 accounts for about one-half of the total energy for N_2 adsorption on Na/X zeolite, as shown in Table I. The $\phi_{\dot{F}\mu}$ energy for O_2 is approximately one-fourth of that for N_2 (see Eq. (8)).

D. BASIC CONSIDERATIONS FOR SORBENT DESIGN

1. Polarizability (α), Electronic Charge (q), and van der Waals Radius (r)

For van der Waals (dispersion) interactions, the polarizabilities of the sorbate molecule and the atoms on the sorbent surface are both important (see Eq. (9)). For electrostatic interactions, for a given sorbate molecule, the charges and van der Waals radii of the surface atoms are important. The roles of these parameters are discussed separately.

TABLE II
POLARIZABILITIES (α) OF GROUND-STATE ATOMS AND IONS (IN 10^{-24} cm^3)

Atom	α	Atom	α	Atom	α
C	1.76	Li	24.3	Al	6.8
N	1.10	Na	24.08	Si	5.38
O	0.802	K	43.4	Fe	8.4
F	0.557	Rb	47.3	Co	7.5
S	2.90	Cs	59.6	Ni	6.8
Cl	2.18	Mg	10.6		
Br	3.05	Ca	22.8	Li^+	0.029
I	5.35	Sr	27.6	Na^+	0.180
		Ba	39.7	K^+	0.840
				Ca^{2+}	0.471
				Sr^{2+}	0.863
				Ba^{2+}	1.560

For a given sorbate molecule, its dispersion interaction potential with a surface atom increases with the polarizability of that surface atom. The polarizability increases with atomic weight for elements in the same family, whereas it decreases with increasing atomic weight for elements in the same row of the periodic table as the outer-shell orbitals are being increasingly filled. The polarizabilities of selected atoms are given in Table II. It is seen that the alkali and alkaline earth metal atoms have very high polarizabilities. Hence these elements, when present on the surface, can cause high dispersion potentials. When these elements are present as cations, however, the polarizabilities are drastically reduced. The polarizabilities of selected cations are also included in Table II for comparison.

For electrostatic interactions, the charges (q) and the van der Waals radii of the surface atoms (or ions) are most important. For ionic solids with point charges distributed on the surface, the positive and negative fields can partially offset when they are spaced closely. However, anions are normally bigger than cations. Consequently, the surface has a negative electric field. All electrostatic interaction potentials are proportional to q ($\Phi_{F\mu}$ and Φ_{FQ}) or q^2 (Φ_{Ind}) and inversely proportional to r^n (where $n = 2$, 3, 4; see Eqs. 6–8). Here r is the distance between the centers of the interacting pair, which should be the sum of the van der Waals radii of the two interacting atoms. Hence the van der Waals radii of the ions on the surface are important. The strong effects of charge (q) and ionic radius of the cation on the adsorption properties of ion-exchanged zeolites are discussed in a later section.

Because the ionic radius determines the distance r, it has a strong effect on the electrostatic interactions. The ionic radii of selected cations are given in Table III.

TABLE III
IONIC RADII, r_i (Å)

Ion	r_i	Ion	r_i
Li^+	0.68	Al^{3+}	0.51
Na^+	0.97	Ce^{3+}	1.03
K^+	1.33	Cu^{+1}	0.96
Rb^+	1.47	Cu^{2+}	0.72
Cs^+	1.67	Ag^+	1.26
Mg^{2+}	0.66	Ag^{2+}	0.89
Ca^{2+}	0.99	Au^{+1}	1.37
Sr^{2+}	1.12	Ni^{2+}	0.69
Ba^{2+}	1.34	Ni^{3+}	0.62

2. Pore Size and Geometry

The potentials discussed previously are those between two molecules or atoms. The interactions between a molecule and a flat, solid surface are greater because the molecule interacts with all adjacent atoms on the surface, and these interactions are assumed pairwise additive. When a molecule is placed between two flat surfaces, i.e., in a slit-shaped pore, it interacts with both surfaces, and the potentials on the two surfaces overlap. The extent of the overlap depends on the pore size. For cylindrical and spherical pores, the potentials are still greater because more surface atoms interact with the adsorbate molecule.

The effects of the pore size and pore geometry are best illustrated by Table IV. Table IV lists the threshold pressure for adsorption in different pore sizes and geometries for N_2 on carbon. The calculation was based on

TABLE IV
THRESHOLD PRESSURE FOR ADSORPTION IN DIFFERENT PORE SIZES AND SHAPES; N_2 ON CARBON AT 77 K; $P_0 = 1$ ATM

Pore size (Å)	P/P_0 for slit shape	P/P_0 for cylindrical shape	P/P_0 for spherical shape
3	6.7×10^{-9}	1.1×10^{-13}	5.4×10^{-52}
4	6.3×10^{-7}	1.3×10^{-12}	3.2×10^{-51}
5	9.1×10^{-6}	2.9×10^{-10}	1.1×10^{-42}
6	3.5×10^{-5}	8.3×10^{-9}	2.5×10^{-36}
7	1.2×10^{-4}	6.5×10^{-8}	6.2×10^{-32}
9	6.1×10^{-4}	3.5×10^{-6}	3.1×10^{-24}
12	2.6×10^{-3}	2.3×10^{-5}	1.2×10^{-20}
15	6.1×10^{-3}	3.2×10^{-4}	1.7×10^{-16}
20	1.4×10^{-2}	1.2×10^{-3}	6.1×10^{-13}

the Horvath–Kawazoe (HK) model (Horvath and Kawazoe, 1983), using the corrected version by Rege and Yang (2000). The corrected HK model has been shown to give pore dimensions from N_2 isotherms that agreed well with the actual pore dimension for a number of materials, including carbon and zeolites (Rege and Yang, 2000). The model is based on equating the work done for adsorption (Eq.(1)) to the total sorbate–sorbent and sorbate–sorbate interactions. The latter was the sum with all sorbate surface atoms using the Lennard–Jones potentials The results in Table IV exhibit the remarkable attraction forces acting on the adsorbate molecule due the overlapping potentials from the surrounding walls. The same carbon atom density on the surface was assumed for all geometries, i.e., 3.7×10^{15} l/cm^2. The experimental data on two molecular-sieve carbons agreed with predictions for slit-shaped pores. No experimental data are available for cylindrical pores and spherical pores of carbon. Data on these shapes may become available with the availability of carbon nanotubes and fullerenes (if an opening to the fullerene can be made).

As expected, the total interaction energies depend strongly on the van der Waals radii (of both sorbate and sorbent atoms) and the surface densities. This is true for both HK type models (Saito and Foley, 1991; Cheng and Yang, 1994) and more detailed statistical thermodynamics (or molecular simulation) approaches (such as Monte Carlo and density functional theory). Knowing the interaction potential, molecular simulation techniques enable the calculation of adsorption isotherms (see, for example, Razmus and Hall, (1991) and Cracknell *et al.* (1995)).

III. Activated Carbon, Activated Alumina, and Silica Gel

Activated carbon is the most widely used sorbent. Its manufacture and use date back to the 19th century (Jankowska, Swiatkowski, and Choma, 1991). The pore-size distribution of a typical activated carbon is given in Fig. 1, along with several other sorbents. Excellent reviews on activated carbon are available elsewhere (Jankowska, Swiatkowski, and Choma, 1991; Rouquerol, Rouquerol, and Sing, 1999; Barton *et al.,* 1999).

The raw materials for activated carbon are carbonaceous matters, such as wood, peat, coals, petroleum coke, bones, coconut shells, and fruit nuts. Anthracite and bituminous coals have been the major sources. Starting with the initial pores present in the raw material, more pores, with desired size distributions, are created by the so-called activation process. After initial treatment and pelletizing, one activation process involves carbonization at

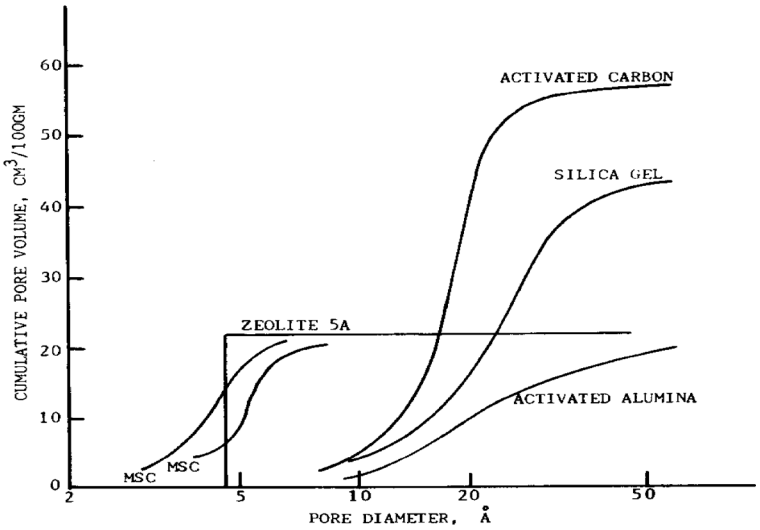

FIG. 1. Pore-size distribution for activated carbon, silica gel, activated alumina, two molecular-sieve carbons, and zeolite 5A (Yang, 1997).

400–500°C to eliminate the bulk of the volatile matter and then partial gasification at 800–1000°C to develop the porosity and surface area. A mild oxidizing gas such as CO_2 steam, or flue gas, is used in the gasification step because the intrinsic surface reaction rate is much slower than the pore diffusion rate, thereby assuring the uniform development of pores throughout the pellet. The activation process is usually carried out in fixed beds, but in recent years fluidized beds have also been used. The activated carbon created by the activation process is used primarily for the gas and vapor adsorption processes. The other activation process that is used commercially depends on the action of inorganic additives to degrade and dehydrate the cellulosic materials and, simultaneously, to prevent shrinkage during carbonization. Lignin, usually the raw material that is blended with activators such as phosphoric acid, zinc chloride, potassium sulfide, or potassium thiocyanate, is carbonized at temperatures up to 900°C. The product, usually in powder form, is used for aqueous- or gas-phase purposes. The inorganic material contained in activated carbon is measured as ash content, generally in the range between 2 and 10%.

By judicious choice of the precursor and also careful control of both carbonization and activation steps, it is possible to tailor the pore structure for particular applications (Barton *et al.,* 1999). There is now a reasonable understanding of the carbonization and activation processes (Barton *et al.,* 1999).

Mesoporosity (near or larger than 30 Å) is desirable for liquid phase applications, whereas smaller pore sizes (10 to 25 Å) are required for gas-phase applications (Yang, 1997).

The unique surface property of activated carbon, in contrast to the other major sorbents, is that its surface is nonpolar or only slightly polar as a result of the surface oxide groups and inorganic impurities. This unique property gives activated carbon the following advantages:

1. It is the only commercial sorbent used to perform separation and purification processes without requiring prior stringent moisture removal, such as is needed in air purification. (It is also useful in aqueous processes.)
2. Because of its large accessible internal surface, it adsorbs more nonpolar and weakly polar organic molecules than other sorbents do.
3. The heat of adsorption, or bond strength, is generally lower on activated carbon than on other sorbents. Consequently, stripping of the adsorbed molecules is easier and results in lower energy requirements for regeneration of the sorbent.

It is not correct, however, to regard activated carbon as hydrophobic. The equilibrium sorption of water vapor on an anthracite-derived activated carbon is compared with that of other sorbents in Fig. 2. The sorption of water vapor on activated carbon follows a Type V isotherm (according to

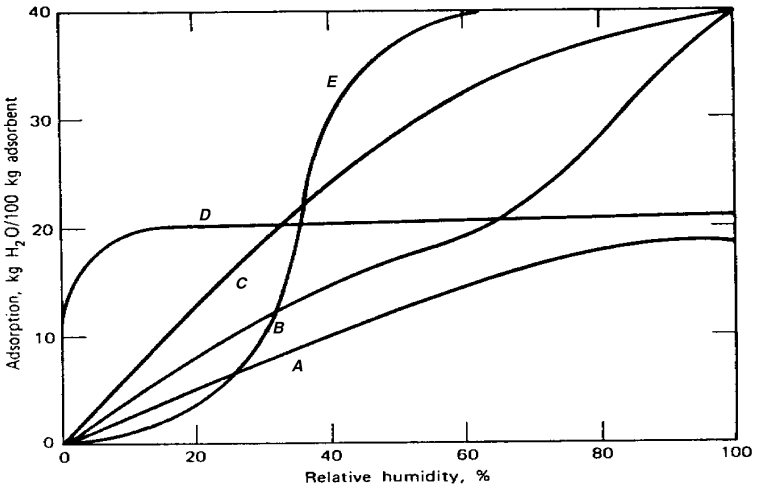

FIG. 2. Equilibrium sorption of water vapor from atmospheric air at 25°C on (*A*) alumina (granular); (*B*) alumina (spherical); (*C*) silica gel; (*D*) 5A Zeolite; and (*E*) activated carbon. The vapor pressure at 100% R.H. is 23.6 Torr (Yang, 1997).

the BDDT classification (Yang, 1997)) due to pore filling or capillary condensation in the micropores. Activated carbon is used, nonetheless, in processes dealing with humid gas mixtures and water solutions because the organic and nonpolar or weakly polar compounds adsorb more strongly, and hence preferentially, on its surface than water does.

A. Recent Developments on Activated Carbon

Interesting developments on activated carbon have been reported recently. They include chemical modification of the surfaces, activated carbon fibers (ACF), and CH_4 and H_2 storage. A brief discussion is given next.

Adsorption of water vapor on activated carbon has been studied extensively because of its scientific as well as practical importance. Chemical modification can significantly alter the adsorption behavior. It has long been known that oxidation and reduction affect the *hydrophobicity* of carbon. The water isotherm generally follows an S-shaped curve, with little or no adsorption at P/P_0 below 0.3 or 0.4. In this region, water molecules are bonded to certain oxygen complexes, likely by hydrogen bonding and electrostatic forces (the nonspecific interactions by Lennard–Jones 6–12 potential are insignificant). At higher P/P_0, clusters and eventually pore filling occur through hydrogen bonding. Pore structure comes into play only in the latter stage. Oxidation of the surface increases the oxygen complexes and hence shifts the threshold P/P_0 for water adsorption. The extensive literature on this subject has been discussed elsewhere (Jankowska, Swiatkowski, and Choma, 1991; Rouquerol, Rouquerol, and Sing, 1999; Leon y Leon and Radovic, 1992; Rodriquez-Reinoso, Molina-Sabio, and Munecas, 1992; Carrasco-Marin *et al.,* 1997; Salame and Bandosz, 1999).

Although the effects of oxidation on water adsorption are expected, the effects of incorporation with other atoms are quite unexpected. Mild chlorination of the surface of activated carbon results in slightly more hydrophobicity (Hall and Holmes, 1993). Mild fluorination has shown drastically increased hydrophobicity, even at $P/P_0 \approx 1$ (Kaneko, Ohbu *et al.,* 1995; Kaneko, Yang *et al.,* 2000). The work on fluorination by Kaneko and colleagues was done on active carbon fibers(ACFs), but their observations are expected on activated carbon as well. Incorporation of nitrogen atoms on ACFs, on the contrary, decreased the hydrophobicity (Kaneko, Yang *et al.,* 2000). A further understanding of the different effects by different chemical modifications is clearly needed.

Activated carbon fibers were a remarkable technological development. The ACFs have high mechanical strengths, high surface areas ($\approx 1000\ m^2/g$), and microporosity (8-10 Å pore dimension) and can be formed into cloth.

High-strength carbon fibers have been produced since 1950s, but ACFs have been available commercially only recently. An activation step is necessary starting from the carbon fibers. Excellent reviews of the development of and studies on ACFs have been made by Suzuki (1994) and Rouquerol, Rouquerol and Sing (1999). Many possible novel applications of the ACF's have been reported (Suzuki, 1994; Kaneko, 2000).

Energy storage, i.e., storage of methane and hydrogen, has attracted much interest, particularly for onboard-vehicle applications. Activated carbon has been the most promising candidate as the sorbent for both methane and hydrogen storage.

Methane cannot be liquefied at ambient temperature ($T_c = 190.6$ K); hence, very high pressures (typically up to 25 MPa) are needed for the requirement of onboard storage. The pressure can be reduced by using sorbents. This subject has been investigated since the early 1980s (Talu, 1993). The target pressure for storage is 4 MPa. The interaction between methane and carbon is only by nonspecific dispersion forces. Among all activated carbons that have been investigated, the storage capacity is approximately proportional to the BET surface area. This proportionality is due to the wide pore-size distribution in the commercial activated carbons. Molecular simulations, however, showed that there is an optimal pore size (assuming slit-shaped pores) for maximum storage (Matranga, Myers, and Glandt, 1992; Jiang, Zollweg, and Gubbins, 1994). which is near 11 Å. Indeed, activated carbon fibers, which have relatively uniform pore sizes (near 10 Å), yielded higher methane-sorption capacities than activated carbons (Alcaniz-Monge *et al.,* 1997). The best carbons have capacities near 200 NTP v/v at 4 MPa at ambient temperature, which is quite adequate for onboard-vehicle applications. The effects of typical impurities that are contained in the natural gas on the charge–discharge behavior have been analyzed (Mota, 1999).

Interests in hydrogen storage by adsorption were intensified only recently. There are four possibilities for onboard hydrogen storage: compressed gas, liquefaction, metal hydrides, and adsorption. Limits on the first three are now well defined. This is not the case with adsorption. Recent claims on hydrogen adsorption in carbon nanotubes have stimulated intense interest (as well as suspicion), which will be discussed separately. The target of 5% (by weight) of storage capacity at 100 atm (and ambient temperature) has been set by the Department of Energy for sorbent development (Yang, 2000). With a typical commercial activated carbon, the amounts adsorbed at 293 K were 0.5% (weight) at 100 atm and 0.32% (weight) at 50 atm (Lamari, Aoufi, and Malbrunot, 2000). However, as environmental concerns and interest in fuel-cell technology increase, the target for hydrogen storage capacity will undoubtedly be lowered. With modifications, activated carbon or ACF could potentially meet the needs.

B. Activated Alumina and Silica Gel

Alumina, silica and many other metal oxides are insulators. However, recent experiments indicate that the surfaces of these insulators are mainly ionic (Masel, 1996). The pristine or freshly cleaved surfaces of single crystals of these oxides (cleaved under ultrahigh vacuum) are fairly inert and do not have significant adsorption capacities for even polar molecules such as CO and SO_2 (Masel, 1996; Henrich and Cox, 1994). However, the surface chemistry and adsorption properties are dominated by defects on real surfaces. For example, oxide vacancies on alumina expose the unsaturated aluminum atoms, which are electron acceptors, or Lewis acid sites.

The commercial alumina and silica gel sorbents are mesoporous, i.e., with pores mostly larger than 20 Å (see Fig. 1). Activated alumina is produced by thermal dehydration or activation of aluminum trihydroxide, $Al(OH)_3$ (Yang, 1997), and is crystalline. Commercially, silica is prepared by mixing a sodium silicate solution with a mineral acid such as sulfuric or hydrochloric acid. The reaction produces a concentrated dispersion of finely divided particles of hydrated SiO_2, known as silica hydrosol or silicic acid:

$$Na_2SiO_3 + 2HCL + nH_2O \rightarrow 2NaCl + SiO_2 \bullet nH_2O + H_2O. \qquad (11)$$

The hydrosol, on standing, polymerizes into a white jellylike precipitate, which is silica gel. The resulting gel is washed, dried and activated. Various silica gels with a wide range of properties such as surface area, pore volume, and strength can be made by varying the silica concentration, temperature, pH, and activation temperature (Iler, 1979). Two typical types of silica gel are known as regular-density and low-density silica gels, although they have the same densities (true and bulk). The regular-density gel has a surface area of 750–850 m^2/g and an average pore diameter of 22–26 Å, whereas the respective values for the low-density gel are 300–350 m^2/g and 100–150 Å.

The silica gel is amorphous. Using high-resolution electron microscopy, it is known that its amorphous framework is made up of small globular (primary) particles having sizes of 10 to 20 Å (Rouquerol, Rouquerol and Sing, 1999). An alternative route involves reactions of silicon alkoxides with water, and a wide variety of materials can be made this way (Jones 1989; Brinker and Sherer, 1990). The processes based on this route are referred to as *sol-gel processing,* and they offer many promising possibilities. For silica gel, the reaction is

$$Si(OR)_4 + 2H_2O \xrightarrow{ROH} SiO_2 + 4ROH. \qquad (12)$$

Silicic acids are also formed by hydrolysis:

$$-\overset{|}{\underset{|}{\text{Si}}}-\text{OR} + \text{H}_2\text{O} \;=\; -\overset{|}{\underset{|}{\text{Si}}}-\text{OH} + \text{ROH} \tag{13}$$

The silicic acids thus formed can then polymerize via

$$-\overset{|}{\underset{|}{\text{Si}}}-\text{OH} + \text{HO}-\overset{|}{\underset{|}{\text{Si}}}- = -\overset{|}{\underset{|}{\text{Si}}}-\text{O}-\overset{|}{\underset{|}{\text{Si}}}- + \text{H}_2\text{O} \tag{14}$$

or

$$-\overset{|}{\underset{|}{\text{Si}}}-\text{OH} + \text{RO}-\overset{|}{\underset{|}{\text{Si}}}- = -\overset{|}{\underset{|}{\text{Si}}}-\text{O}-\overset{|}{\underset{|}{\text{Si}}}- + \text{ROH} \tag{15}$$

The reaction products are high-molecular-weight polysilicates (a sol), which form a three-dimensional porous network filled with solvent molecules (a gel). The more recent development of MCM-41 (to be discussed separately) is a derivative of the sol-gel route. The pore structure, as well as the surface chemistry, can be tailored in the sol-gel route. The pH value in the initial stages (Reactions 13–15) is a main factor in controlling the pore dimensions. Low pH (e.g., by adding HCl) leads to microporosity, whereas high pH (e.g., by adding ammonium hydroxide) results in mesoporosity (Brinker and Sherer, 1990). Apparently, pH influences the size distribution of the globular, primary particles and also how these particles agglomerate and, hence, the final pore structure. Sol-gel processing is highly versatile. It is not limited to silica; it is also applicable to many other main-group and transition metal oxides.

IV. MCM-41

Beck *et al.* (1992) succeeded in the synthesis of a new family of ordered, mesoporous silicate/aluminosilicate by hydrothermal formation of silica gels in the presence of surfactant templates. Typically, quaternary ammonium surfactants were used. The surfactants self-assemble to form micellar templates with a three-dimensional, long-range order. The silicate precursors condense on the walls of the template. The organic templates are subsequently removed by air oxidation, leaving behind a silicate structure. These materials are amorphous but exhibit simple X-ray diffraction patterns ($2\theta = 2^\circ$) that reflect the interplanar spacing of the regular mesoporous structure of the templates. These materials were named M41S, and the materials that have the honeycomb-shaped structures are named MCM-41. A schematic of the formation of MCM-41 is shown in Fig. 3.

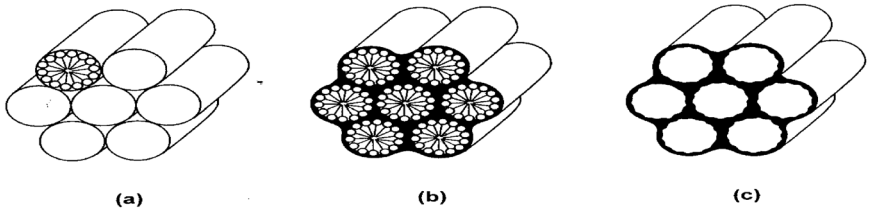

FIG. 3. Schematic representation of the formation of MCM-41 by the liquid-crystal templating mechanism. (a) Hexagonal array of cylindrical micelles; (b) the same, with silicate species between the cylinders; and (c) hollow cylinders of MCM-41 after thermal elimination of organic material. (Rouquerol, Rouquerol and Sing, 1999).

Different mechanisms for the interactions between the silicate precursors and the organic template as well as the liquid crystal templating mechanisms have been discussed (Ying, Mehnert, and Wong, 1999; Tanev and Pinnavaia, 1995). Two other major types of M41S materials are MCM-48 (with 3-D pores) and MCM-50 (with a pillared layer structure).

Among the M41S materials, MCM-41 has received most attention because of its simple structure as well as the ease of synthesis and tailoring of its structure and surface properties. The pore dimension is in the range of 20 to 100 Å and can be tailored by several different strategies (Rouquerol, Rouquerol and Sing, 1999; Ying, Mehnert, and Wong, 1999; Zhao, Lu, and Millar, 1996). The first one is to use surfactants with different chain lengths, and pore diameters can be controlled from near 15 A to 45 Å (Huo, Mragolese, and Stucky, 1996). The use of two surfactants can extend the pore sizes to 55 Å (Kaman, Anderson, and Brinker, 1996). The addition of expander molecules such as trimethylbenzene (Beck *et al.,* 1992; Zhao, Lu, and Millar, 1996) extends the pore size to near 100 Å. Good quality, large pore MCM-41 with pore sizes up to 65 Å can be made by postsynthesis hydrothermal restructuring (Huo, Mragolese, and Stucky, 1996; Sayari *et al.,* 1997). Ordered, nanostructured materials with even larger pores (up to 300 Å) can be obtained by using block copolymers as the structure-directing agents (Zhao *et al.,* 1998). Moreover, MCM-41 with heteroatoms (such as Ti, B and V) and many non-silica materials with structures similar to MCM-41 can be synthesized (Ying, Mehnert, and Wong, 1999; Sun and Ying, 1997).

The unique feature of MCM-41 is the large uniform pore structure (and hence remarkably large pore volume, above 0.7 cm^3/g). This unique feature has made these materials promising for catalysis (as discussed by Ying and colleagues (1999)). However, this unique feature is not attractive for gas adsorption because the interaction potentials are not enhanced within the pores, as discussed earlier. Consequently, relatively few studies have been made on MCM-41 as adsorbents.

In order to obtain useful adsorption properties, MCM-41 needs to be modified in either surface chemistry or pore structure. The reported modifications have been based mainly on the use of reactive silanes that contain organic groups (such as alkyls) and chloride. The formed MCM-41 has hydroxyl groups, and by reacting the hydroxyl group with silanes, i.e. silanation, pore sizes can be reduced by the grafted silanes (Feng *et al.,* 1997; Jaroniec *et al.,* 1998). The grafting can be accomplished by many other compounds such as metal alkoxides and halides, hence the chemistry of the surface can be altered or functionalized (Moller and Bein, 1998; Jaroniec *et al.,* 1998). Functionalization of the surface can be also accomplished before the final calcination step by directly displacing the sulfactants with reactive silanes (Antochsuk and Jaroniec, 2000). A technique to reduce the pore size only at the opening regions has been suggested (Zhao, Lue, and Hu, 1999), by grafting a controlled number of layers of silica in the opening regions. This was done by displacing the surfactant in the opening regions by H^+, followed by silanation with $Si(OEt)_4$ and hydrolysis, and finally calcination.

Only few promising applications of the MCM-41 and its modified forms have been reported. Izumi and coworkers have reported the use of MCM-41 for VOC removal (Izumi, 1996) and SO_2 removal (Teraoka *et al.,* 2000), by taking advantage of the weak bonds with the surface and, hence, ease in desorption. They also reported a low-temperature synthesis route for MCM-41 at very low pH (<1), which is a possible low-cost method. Feng *et al.* (1997) grafted the MCM-41 with a silane-containing thiol ($-$SH) group and produced a sorbent that is highly selective for binding heavy metal ions such as mercury, silver, and lead ions from wastewaters. The sorbent is also regenerable with HCl. Because of the large arrays of functionalities and pore sizes that can be achieved with the MCM-41 material, unique adsorption properties will no doubt be obtained. However, due to the cost, its use appears to be limited to specialized applications.

V. Zeolites

Zeolites are crystalline aluminosilicates of alkali or alkali earth elements such as sodium, potassium, and calcium and are represented by the stoichiometry:

$$M_{x/n}\,[(AlO_2)_x(SiO_2)_y]\,zH_2O,$$

where x and y are integers, with $y/x \geq 1$, n is the valence of cation M, and z is the number of water molecules in each *unit cell*. Unit cells are shown in Fig. 4(b) and (c). The cations are necessary to balance the electrical charge

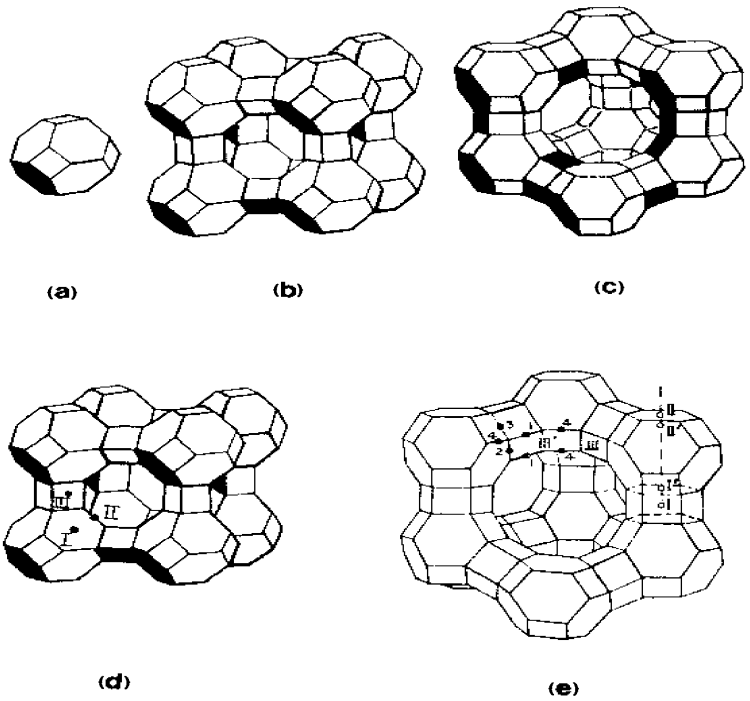

FIG. 4. Line representations of zeolite structure: (a) sodalite cage, or truncated octahedron; (b) type A zeolite unit cell; (c) unit cell of types X and Y, or faujasite; (d) cation sites in type A (there are 8 I, 3 II, and 12 III sites per unit cell); (e) cation sites in types X and Y (16 I, 32 I′, 32 II, 32 II′, 48 III, and 32 III′, sites per unit cell).

of the aluminum atoms, each having a net charge of –1. The water molecules can be removed with ease upon heat and evacuation, leaving an almost unaltered aluminosilicate skeleton with a void fraction between 0.2 and 0.5. The skeleton has a regular structure of cages, which are usually interconnected by six windows in each cage. The cages can imbide or occlude large amounts of guest molecules in place of water. The size of the window apertures, which can be controlled by fixing the type and number of cations, ranges from 3 Å to 10 Å . The sorption may occur with great selectivity because of the size of the aperature (and to a lesser extent because of the surface property in the cages)—hence the name *molecular sieve*.

At least 40 species of naturally occurring zeolites have been found. The principal ones are chabazite, $(Ca, Na_2)Al_2Si_4O_{12}(6\,H_2O)$; gmelinite, (Na_2, Ca) $Al_2Si_4O_{12}(6\ H_2O)$; mordenite, $(Ca, K_2, Na_2)Al_2Si_{10}O_{24}(6.66\ H_2O)$; levynite, $Ca,Al_2Si_3O_{10}(5\ H_2O)$; and faujasite, $(Na_2, Ca, Mg, K_2)OAl_2Si_{4.5}O_{12}$ $(7\ H_2O)$. More than 150 types of zeolites have been sythesized; they are designated by

a letter or group of letters: Type A, Type X, Type Y, Type ZSM, and so on. The commercial production of synthetic zeolites started with the successful development of low-temperature (25–100°C) synthesis methods using very reactive materials such as freshly coprecipitated gels or amorphous solids (Breck, 1974; Milton, 1959). Two comprehensive monographs, by Barrer (1978) and Breck (1974), deal with all aspects of zeolites. The zeolites that have been synthesized more recently are discussed by Szostak (1998).

A. Structures and Cation Sites

The primary structural units of zeolites are the tetrahedra of silicon and aluminum, SiO_4 and $A1O_4$. These units are assembled into secondary polyhedral building units such as cubes, hexagonal prisms, octahedra, and truncated octahedra. The silicon and aluminum atoms, located at the corners of the polyhedra, are joined by a shared oxygen. The final zeolite structure consists of assemblages of the secondary units in a regular three-dimensional crystalline framework. The ratio Si/Al is commonly 1 : 5. The aluminum atom can be removed and replaced by silicon in some zeolites, thereby reducing the number of cations, and the cations can also be exchanged. The inner atoms in the windows are oxygen. The size of the windows depends, then, on the number of oxygen atoms in the ring—four, five, six, eight, ten or twelve. The aperture size, as well as the adsorptive properties, can be further modified by the number and type of exchanged cations. A description of the structures will be given only for the zeolites important in gas separation—Type A and Types X and Y.

1. Type A

The structural unit in Type A zeolite, as well as that in Types X and Y, is the truncated octahedron, shown in Fig. 4(a). This unit is also called a sodalite cage, because sodalite is formed by directly fusing the four-member rings of the units. The four-member rings of the sodalite units can also be linked through four-member prisms, as shown in Fig. 4(b), which is Type A zeolite. The unit cell of Type A zeolite, as shown in this figure, contains 24 tetrahedra, 12 AlO_4, and 12 SiO_4. When fully hydrated, 27 water molecules are contained in the central cage, or cavity, of the unit cell and in the eight smaller sodalite cages. The free diameter in the central cavity is 11.4 Å, which is entered through six eight-member oxygen-ring apertures with a minimum diameter of 4.4 Å. There are 12 negative charges to be balanced by cations in each unit cell. The most probable locations for the cations are indicated in Fig. 4(d). Type I is at the center of the six-member ring and thus at one of the eight

corners of the cavity. Type II is at the eight-member aperture, directly obstructing the entrance. Type III is near the four-member ring inside the cavity.

Type A zeolites are synthesized in the sodium form, with 12 sodium cations occupying all eight sites in I and three sites in II, plus one site in III. This is the commercial Type 4A zeolite, with an effective aperture size of 3.8 Å. The sodium form can be replaced by various other cations or by a hydrogen ion. The commercial Type 3A zeolite is formed by exchanging Na^+ with K^+, resulting in a smaller effective aperture size due to the larger K^+. The aperture size of the sodium form can also be increased by exchanging Na^+ with Ca^{+2} or Mg^{+2}, because 2 Na^+ are replaced by one divalent cation. The form of the exchanged Ca^{+2} or Mg^{+2} is Type 5A with rather unobstructed and larger apertures.

2. Types X and Y

The skeletal structure of Types X and Y zeolites is the same as that of the naturally occurring faujasite. The sodalite units are linked through six-member prisms, as shown in the unit cell in Fig. 4(c). Each unit cell contains 192 $(Si, Al)O_4$ tetrahedra. The number of aluminum ions per unit cell varies from 96 to 77 for Type X zeolite and from 76 to 48 for Type Y zeolite. This framework has the largest central cavity volume of any known zeolite, amounting to about 50% void fraction in the dehydrated form. A unit cell, when fully hydrated, contains approximately 235 water molecules, mostly in the central cavity. The aperture is formed by the 12-member oxygen rings with a free diameter of approximately 7.4 Å. Three major locations for the cations are indicated in Fig. 4(e). The locations are center of the six-member prism (I) and opposite to I in the sodalite cage (I′); similar to I and I′ but further from the central cavity (II and II′); and the 12-member aperture (III and III′). The commercial 10X zeolite contains Ca^{+2} as the major cation, and Na^+ is the major cation for 13X zeolite. The distribution of Na^+, K^+, Ca^{+2}, other cations, and H_2O among the sites in X and Y zeolites has been discussed in detail by Barrer (1978). The BET surface are a measured with N_2 for zeolites falls in the range between 500 and 800 m^2/g.

B. Unique Adsorption Properties: Anionic Oxygens and Isolated Cations

Zeolites exhibit many unique adsorption properties, mainly because of their unique surface chemistry. The surface of the framework is essentially oxygen atoms, because Si and Al are buried or recessed in the tetrahedra of oxygen atoms, so they are not exposed and cannot be accessed by adsorbate molecules. Also, the anionic oxygen atoms are much more polarizable

than the Al and Si cations, as well as being more abundant. Therefore, the numerous and anionic oxygen atoms dominate the van der Waals interactions with the sorbate molecules, i.e., $\phi_D + \phi_R$(dispersion + repulsion).

Besides the anionic oxygen, cations are located at certain sites, and most of these sites are hidden or inaccessible to the adsorbate molecules. However, with molecules with permanent dipoles and quadrupoles, the interactions with these few exposed cations can dominate the total interaction potential.

The anionic surface oxygens carry negative charges, and the charge depends on the location of the oxygen relative to the cation sites and also on the cation. In Monte Carlo simulations, a constant charge is usually assigned to all surface oxygen atoms and the value is usually determined by fitting the experimental data (of isosteric heat of adsorption or the isotherm). For example, a charge of $-1/3$ was used by Razmus and Hall (1991) and -1.2 was used by Mellot and Lignieres (1997).

It is instructive to compare the relative electronegativities of the anion of the zeolite framework with simple anions such as halides. Such a comparison can be made by calculating the net charges of the anions (or cations) using molecular orbital theories. The Gaussian 94 Program in Cerius[2] molecular modeling software from Molecular Simulations, Inc., was used for the calculation (Takahashi, Yang, and Yang, 2000; Yang and Yang, unpublished). The calculations were performed at the Hartree–Fock (HF) and density functional theory (DFT) levels using effective core potentials (ECPs). The LanL2DZ basis set was employed for both geometry optimization and natural bond orbital (NBO) analysis. The net charges were calculated by using NBO. The zeolite model used in the calculation was the cluster model shown in Fig. 5. The results are shown in Table V.

From Table V, the zeolite anion is more electronegative than F^-. Also shown in Table V are the electron occupancies in the 5*s* orbital of the Ag^+ that is bonded to the anion. For a perfect anion, the Ag^+ to which it is bonded should have an empty 5*s* orbital. Again, it is seen that Ag^+ in AgZ has the lowest occupancy in its 5*s* orbital, indicating that the Z^- (i.e., zeolite framework anion) is the most electronegative anion.

The strong anionic nature of the zeolite framework and the corresponding, strong cations are unique with zeolites. Furthermore, the cations and anions are not located closely to each other, which exert strong electric fields over the surface.

C. Interactions with Cations: Effects of Site, Charge, and Ionic Radius

In earlier discussions, the strong or dominating contributions of cation–dipole and cation–quadrupole interactions to the total bonding were seen

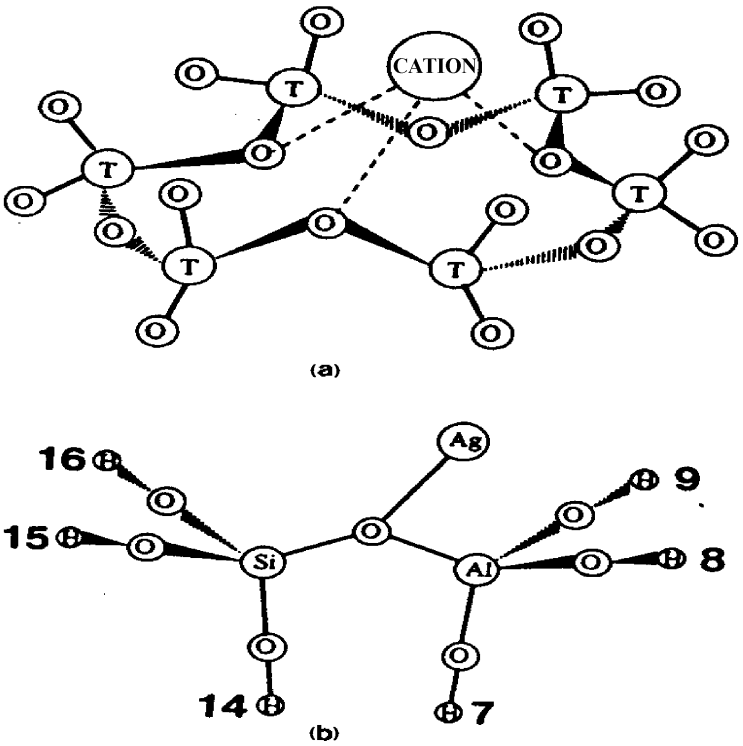

FIG. 5. (a) Site II cation on a six-membered oxygen ring as the basic unit on types A and X zeolites. T denotes Si or Al. (b) Geometry-optimized cluster model to represent the chemistry of Ag/zeolite.

TABLE V

RELATIVE ELECTRONEGATIVITIES OF ZEOLITE ANION AND HALIDES—COMPARISON OF ANION NET CHARGES CALCULATED BY MOLECULAR ORBITAL THEORY USING B3LYP/LANL2DZ WITH NBO METHOD[a]

	Anion charge, electronic unit	Electron occupancy in 5*s* orbital of Ag^+
Ag^+Z^-	0.5765	0.142
Ag^+F^-	0.5111	0.295
Ag^+Cl^-	0.3404	0.357
Ag^+Br^-	0.3017	0.393
Ag^+I^-	0.2375	0.437

[a]AgZ denotes Ag zeolite using the model in Fig. 5.

(see Table I). Unfortunately, except ionic radii, the cation sites and the charges have not been well determined. Hence they remain largely as fitting parameters in molecular simulations. However, the strong effects of these parameters on adsorption are well established.

1. Effects of Cation Sites

Cation sites are well defined in type A zeolite but are not well defined in nearly all other zeolites, including LSX (low silica X, Si/Al $= 1$). Most of the cation sites are hidden and are not accessible for interactions with the adsorbate molecules.

Effects of cation sites can be best illustrated with the important system of N_2/O_2 on type X zeolites. Na/X (or 13X) has been used commercially for air separation since the 1970's. Li/LSX is the best sorbent commercially available today (Chao, 1989). Mixed-cation AgLi/LSX (with 1–3% Ag cations) has been shown to be even better than Li/LSX (Yang and Hutson, 1998; Hutson, Rege, and Yang, 1999).

As shown in Fig. 4, there are 192 possible cation sites in a unit cell of faujasite (or X zeolite). For LSX, there are only 96 cations (monovalent). Upon activation of the zeolite, i.e., heating at 350°C, the cations migrate to the sites with the lowest energies. Migration is an activated process, which depends on the temperature, time, and the size of the cation. Unfortunately, the most stable sites (that have the lowest energies) are the hidden sites, not exposed to the supercage cavity. So relatively few exposed sites are occupied.

By ion exchange of Na^+ with Li^+ in the LSX, Chao (1989) obtained significantly improved N_2/O_2 selectively. This improvement was the result of the smaller ionic radius of Li^+ (0.68 Å) compared to Na^+ (0.97 Å), with equal charge and, hence, much higher $\phi_{\vec{F}Q}$ (electric field gradient–quadrupole) potential. However, no improvement was seen until approximately more than a 70% ion exchange was made, and the selectivity increased linearly with ion exchange beyond this threshold value (see Fig. 6). (Figure 6 actually shows LiX with different Si/Al ratios, or different number of Li cations per unit cell. But it illustrates the same phenomenon.) The reason for this significant phenomenon was that Sites I, I′ and II′ were lower-energy sites, which were preferred by Li^+ (Chao, *et al.,* 1992; Coe, 1995). Sites II and III are exposed sites but have lower coordination and are less preferred. These exposed sites are most important for adsorption.

Although Ag^+ has a larger ionic radius (1.26 Å) than Li^+, we have found that π-complexation bond was formed between Ag^+ (in AgZ) and N_2 (Chen and Yang, 1996). This π-complexation bond, although weak, enhanced the adsorption for N_2 significantly (Yang and Hutson, 1998; Hutson, Rege, and Yang, 1999).

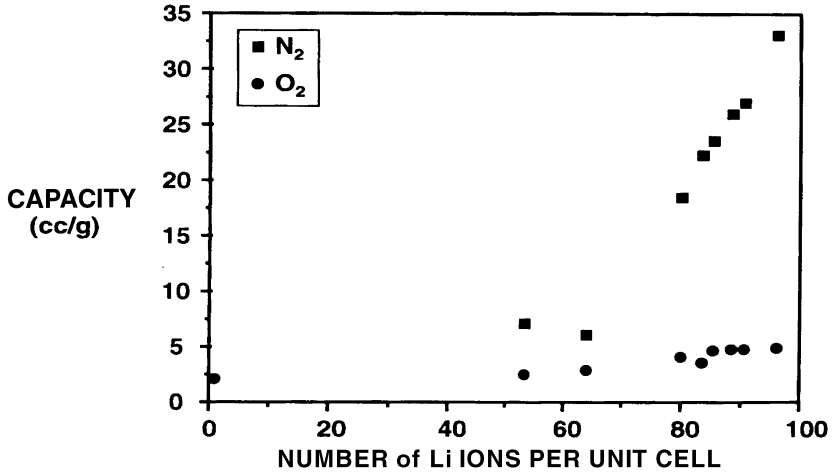

FIG. 6. N_2 and O_2 adsorption capacities at 23°C and 1 atm for Li faujasite with different Si/Al ratios. (Coe, 1995; this result is similar to that given in Chao (1989)).

The pure Ag/LSX (Si/Al = 1) adsorbs 22 nitrogen molecules per unit cell at 1 atm and 25°C. The capacity depends on the temperature of heat treatment, as shown in Fig. 7. X-ray photoelectron spectroscopy (XPS) results showed that some reduction takes place during heating from 350 to 450°C in *vacuo* or in an inert atmosphere. Moreoever, a color change

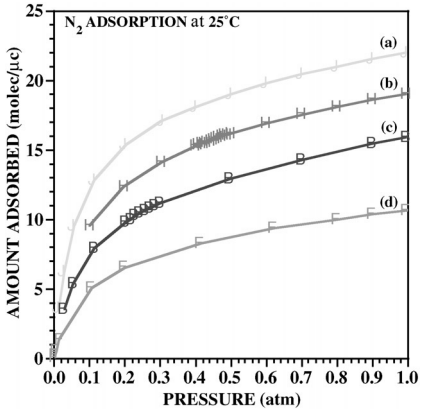

FIG. 7. N_2 adsorption isotherms, measured at 25°C, for Ag/LSX (a) after drying at room temperature followed by vacuum dehydration at 450°C, (b) after drying at room temperature followed by vacuum dehydration at 350°C, (c) after drying in air at 100°C followed by vacuum dehydration at 350°C and (d) after drying in air at 100°C in air, followed by heat treatment in air at 450°C and, finally, vacuum dehydration at 450°C (Hutson and Yang, 2000).

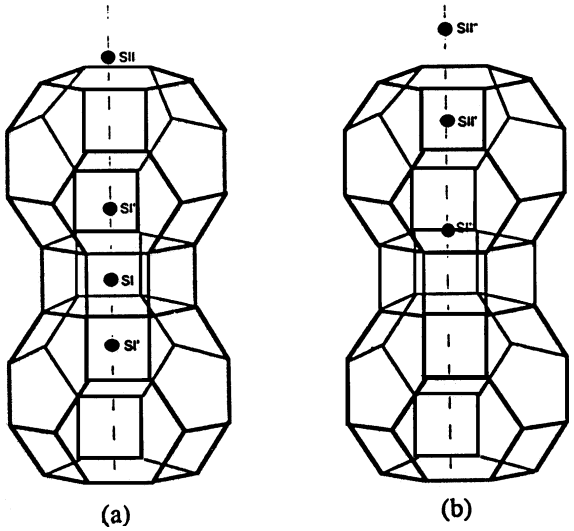

FIG. 8. Sodalite and hexagonal prism site I and II cation locations in Ag/faujasites. Configuration (a) shows the normal cation locations with occupied sites at SI, SI′ and SII. Configuration (b) shows cation sites that have resulted from cation and/or cluster migration upon vacuum thermal treatment. This configuration shows occupied sites at SI′*, SII′, and SII* (Hutson and Yang, 2000).

from white to brick red occurs. These are the result of the formation of trinuclear $Ag^+-Ag^0-Ag^+$ cluster. A detailed neutron diffraction analysis has identified the site of the Ag cluster as shown in Fig. 8. From Fig. 8, it is seen that some of the Ag^+ originally located at site SII (after heating to 350°C) are now located at site SII*. The cation at SII is significantly shielded by the six oxygen atoms o the 5-ring and hence sterically is only partially accessible to the adsorbate N_2. After heating to 450°C, the Ag^+ located at SII* becomes less shielded by the 6 O atoms. Hence, there are more interactions (including weak π-complexation) with nitrogen.

The isosteric heats of adsorption of N_2 on Li/LSX and Ag/LSX are shown in Fig. 9.

In is seen that the first N_2 molecule adsorbed in the unit cell of AG/LSX has a bond energy of about 10 kcal/mol, decreased quickly to below 7 kcal/mol for other N_2 molecules. This difference of 3 kcal/mol is the result of bonding with Ag^+ at Site II*. The vertical distance between SII and SII* is 0.75 Å (Fig. 8). This small difference causes significantly less shielding (by O atoms) and consequently much stronger bonding with the sorbate molecule.

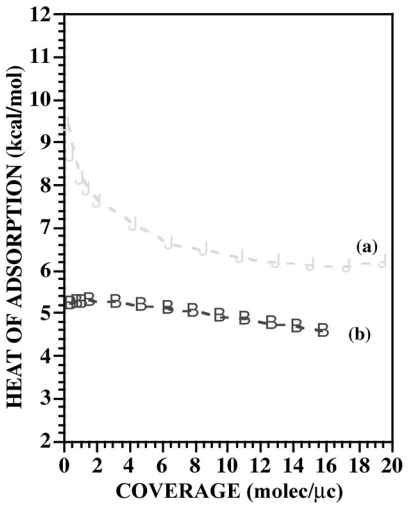

FIG. 9. Heat of adsorption (kcal/mol) versus surface coverage (molec/μc) for N_2 adsorption on (a) Ag-LSX-450 and (b) Li LSX-450.

Another example for illustrating the cation-shielding effect on adsorption is by comparing the N_2 adsorption on NaY and LiY zeolites (Mellot and Lignieres, 1997). The type Y zeolite has the same framework structure as X but with less than 76 cations per unit cell (due to higher Si/A1 ratios). In this case, Site II is the only exposed site for Na^+ and Li^+. LiY is expected to adsorb N_2 more strongly than NaY because of its smaller cations. The experimental isotherms are, however, the same (Mellot and Lignieres, 1997). The reason is that the Li^+ in site II is more shielded by O atoms, as evidenced by a shorter Li^+–O (framework) bond (of 2.07 Å) than the Na^+–O (framework) bond (of 2.48 Å) (Shepelev, Anderson, and Smolin, 1990). Moreover, on the same X zeolite framework, it was necessary to assign different charges for the four Ca^{2+} cations (2, 1.2, 1.2, 1.2) on the four SII sites in order to account for the energetic heterogeneity for N_2 adsorption (Mellot and Lignieres, 1997).

2. Effects of Cation Charge and Ionic Radius

The equilibrium distance between an interacting pair is the sum of the van der Waals or ionic radii of two atoms. Hence the ionic radius of the cation is important in all interactions, both nonspecific and electrostatic interactions. The ionic radii of important cations are listed in Table III. The cationic charge, on the other hand, is important only to the electrostatic interactions.

The effects of cation charge and ionic radius on the interaction energies are best seen in Eqs. (4)–(8). For electrostatic interactions, the following dependence holds:

Induction:

$$\phi_{\text{Ind}} \propto \frac{q^2\alpha}{r^4}. \tag{16}$$

Field-dipole:

$$\phi_{F\mu} \propto \frac{q\mu}{r^2}. \tag{17}$$

Field gradient-quadrupole:

$$\phi_{FQ} \propto \frac{qQ}{r^3}, \tag{18}$$

where

$$r = r_i \text{ (ionic radius)} + r_j\text{(adsorbate atom or molecule)}. \tag{19}$$

Table VI shows the interaction energies of Ar, O_2 and N_2 interacting with isolated cations. For Ar, Eqs. (4)–(8) were used (Barrer and Stuart, 1959). For O_2 and N_2, the values were calculated from quantum mechanics which represent the sum of L–J and electrostatic interactions (Mellot and Lignieres,

TABLE VI
INTERACTION ENERGIES (ϕ) BETWEEN MOLECULES AND ISOLATED CATIONS[a]

Molecule or Ion	r Å	$10^{24}\alpha$ cm^3	Q esu	$-(\phi_D + \phi_R)$ kJ/mol	$-\phi_{\text{Ind}}$ kJ/mol	$-\phi_{\text{total}}$ kJ/mol
Ar	1.92	1.63	0			
O(O_2)	1.73	1.58	−1.3			
N(N_2)	1.89	1.74	−4.7			
Ar-Ion						
Li^+	0.78	0.029	0	0.210	21.3	21.5
Na^+	0.98	0.180	0	0.670	16.0	16.6
K^+	1.33	0.840	0	1.80	10.2	12.0
Ca^{2+}	0.99	0.471	0	2.13	63.5	65.6
Sr^{2+}	1.13	0.863	0	3.26	52.7	55.9
Ba^{2+}	1.35	1.560	0	4.22	40.7	44.9
O_2-Li^+						32
O_2-Na^+						20
N_2-Li^+						51
N_2-Na^+						36

[a]Values for O_2 and N_2 are from Mellot and Lignieres (1997) and all others are from Barrer (1978); Van der Waals radius and ionic radius are denoted by r. N_2-ion and O_2-ion are in linear arrangements.

TABLE VII
COMPONENTS OF INTERACTION ENERGIES (ϕ, IN kJ/mol) FOR CO_2 ADSORBED ON X ZEOLITE WITH DIFFERENT CATIONS[a]

Component	Li	Na	K	Rb	Cs
$-\phi_D$ (Oxygens)	15.9	13.0	7.1	4.6	4.6
$-\phi_D$ (Cations)	0.4	0.8	3.3	4.6	9.2
$-\phi_{\text{Ind}}$	9.6	5.0	2.1	0.8	0
$-\phi_{\bar{F}Q}$	30.9	21.3	17.6	14.6	9.6

[a]CO_2 is oriented along the ppp axis in the cavity (Barrer, 1978; Barrer and Gibbons, 1965); for CO_2: $\mu = 0$ and $Q = -4.3$ ESU.

1997). For Ar-cation pairs, as the cation increases in size, the polarizability increases, and so $(\phi_D + \phi_R)$ also increases. The induction energy, in contrast, decreases sharply with the increasing size, as shown in Eq. (16) ($\propto r^{-4}$). The divalent cations are slightly bigger but have twice the amount of charge; hence, the induction energy increases sharply ($\propto q^2$). For N_2 and O_2 interacting with the same cation, the nonspecific $(\phi_D + \phi_R)$ and ϕ_{Ind} energies are about the same because their sizes, polarizabilities, and magnetic susceptibilities are about the same. The main difference in the total interacting energies comes from $\phi_{\bar{F}Q}$. The substantial differences for the four pairs (O_2–Li^+, O_2–Na^+, N_2–Li^+ and N_2 – Na^+) are clearly seen in Table VI. For O_2 interacting with Li^+ and Na^+, the difference of 12 kJ/mol is caused by the different sizes of the ions (see Eq. (18)). For the same ion with O_2 and N_2, the large difference is caused by the difference in the quadrupole moment. The dependence follows Eq. (18).

Barrer and Gibbons (1965) did calculations for the interaction potentials of CO_2 and NH_3 moving along the axes running through the center of the 12-ring window of faujasite-type 26-hedral cage of zeolite X. The results are shown in Tables VII and VIII. The qualitative comparison with experimental

TABLE VIII
ENERGY TERMS IN kJ/mol FOR NH_3 IN X ZEOLITE WITH DIFFERENT CATIONS (BARRER, 1978; BARRER AND GIBBONS, 1965); FOR NH_3: $\mu = 1.47$ DEBYE AND $Q = -1.0$ ESU

Cation	$-\phi_D$ (Oxygens)	$-\phi_D$ (Cations)	$-\phi_R$	$-\phi_{F\mu}$	$-\phi_{\text{Ind}}$	$-\phi_{\text{total}}$	Expt'l ($-\Delta$H)
Li	47.2	1.7	41.3	50.6	23.0	77.7	76.5
Na	33.8	3.3	23.4	33.0	9.6	53.9	72.3
K	9.6	6.7	14.6	20.1	3.8	23.8	59.8
Rb	7.9	11.7	18.0	17.6	2.9	20.5	55.6
Cs	7.5	16.3	19.6	15.0	2.1	19.6	47.2

data was remarkably good considering the calculations were made about 1965. In Table VII, the quadrupole-field gradient interaction dominates the adsorption of CO_2, because CO_2 has no dipole but has a strong quadrupole. The interaction energy is nearly proportional to r^{-3} (Eq. (18)), showing the strong dependence on the ionic radius of the cation. For NH_3, which has strong dipole and moderately strong quadrupole, the dipole-field interaction is clearly not important (Table VIII). The $\Phi_{F\mu}$ term is proportional to r^{-2} (Eq. (17)). The strong dependence on the cation size is also clearly seen in Table VIII.

A note needs to be made on the interactions with the zeolites with divalent (and higher-valent) cations. The energies of CO_2 on X zeolites with different univalent cations follow the order that larger ions give lower initial heats of adsorption (Table VII and (Barrer, 1978)). For divalent ions, the heats follow the reverse sequence of $Ba^{2+} > Sr^{2+} > Ca^{2+}$ (Barrer, 1978). This is also the case with N_2 adsorption (Mckee, 1964). Both N_2 and CO_2 are nonpolar but highly quadrupolar. For zeolites exchanged with univalent cations, the ϕ_{FQ} term dominates. For divalent cations, however, the large polarizabilities (Table II) become important, and the dispersion and induction energies are large, especially for Ba^{2+}. Hence all interaction terms need to be considered.

VI. π-Complexation Sorbents

All industrial adsorption processes are essentially based on van der Waals and electrostatic interactions between the sorbate and the sorbent. Chemical bonds have yet to be exploited. As suggested by King (1987), chemical complexation bonds are generally stronger than van der Waals interactions (thus giving rise to higher selectivities), yet they are weak enough to be reversible (i.e., to be broken by simple engineering means). This picture is well illustrated by the bond-energy-bond-type diagram of G. E. Keller and colleagues (1992). Indeed, a number of important separations have been proposed by King and coworkers using solvents with functional groups to form reversible chemical complexation bonds between the solute and solvent molecules (King, 1987). The π-complexation is a special class complexation. It pertains to the main group (or *d*-block) transition metals. These metals and their ions can form the usual σ bonds with their *s* orbitals and, in addition, their *d* orbitals can back-donate electron density to the antibonding π orbitals of the molecule that is to be bonded. The π-complexation has been seriously considered for olefin/paraffin separation and purification by employing liquid solutions containing silver (Ag^+) or cuprous (Cu^{+1}) ions

(Quinn, 1971; Ho *et al.,* 1988; Keller *et al.,* 1992; Blytas, 1992; Eldridge, 1993; Safarik and Eldridge, 1998). Although gas–solid operations can be simpler as well as more efficient, particularly by pressure-swing adsorption, the list of attempts for developing solid π-complexation sorbents is a short one (Hirai; Hara, and Komiyama, 1985; Hirai, Kurima, *et al.,* 1985). CuCl, which is insoluble in water, has been considered for olefin–paraffin separations (Gilliand, Bliss, and Kip, 1941; Long, 1972). The only apparently successful solid sorbent of this nature before our work was CuCl/γ-Al_2O_3 for binding with the π bond of CO (Xie and Tang, 1990; Kumar *et al.,* 1993). It should also be noted that the commercially available sorbents do not have significant selectivities for olefins (over corresponding paraffins) and the use of these sorbents would require additional, substantial operations (Kulvaranon, Findley, and Liapis, 1990; Jarvelin and Fair, 1993; Ghosh, Lin, and Hines, 1993).

Efficient solid π-complexation sorbents have been developed within the last 5 years in the author's laboratory (Yang and Kikkinides, 1995; Chen and Yang, 1996; Wu *et al.,* 1999; Rege, Padin, and Yang, 1998; Huang, Padin, and Yang, 1999a, 1999b; Padin, Yang, and Munson, 1999; Padin and Yang, 2000), mainly for olefin–paraffin separations. The bond between the sorbent and the sorbate needs to be strong. However, excessively strong bonds lead to either reaction or irreversible adsorption. Empirically, the adsorption is "reversible" when the bond is below 15 to 20 kcal/mol, i.e., desorption can be achieved easily by simple engineering operations such as pressure and temperature changes. The strength of the bonding between sorbate and sorbent depends on

- Emptiness of the outer-shell *s* orbital of the cation on the sorbent surface
- The amount of π electrons in the target adsorbate molecule and the ease with which to donate to the cation

Molecular orbital theory has been used to study π-complexation (Chen and Yang, 1996; Huang, Padin, and Yang, 1999a, 1999b). Molecular orbital theory can serve as an ideal tool for designing sorbents for π-complexation for a given target adsorbate molecule.

A. π-Complexation Sorbents for Olefin–Paraffin Separations

Olefin–paraffin separations represent a class of most important and also most costly separations in the petrochemical industry. Cryogenic distillation has been used for more than 60 years for these separations (Keller *et al.,* 1992). They remain to be the most energy-intensive distillations because of

the close relative volatilities. The most important olefin–paraffin separations are for the binary mixture of ethane–ethylene and propane–propylene. A number of alternatives have been investigated (Eldridge, 1993; Safarik and Eldridge, 1998). The most promising alternative is separation based on π-complexation.

In our laboratory, several new sorbents based on π-complexation were prepared for selective olefin adsorption. These include Ag^+-exchanged resins (Yang and Kikkinides, 1995; Wu *et al.,* 1999), monolayer $CuCl/\gamma\text{-}Al_2O_3$ (Yang and Kikkinides, 1995), monolayer CuCl on pillared clays (Cheng and Yang, 1995), and monolayer $AgNO_3/SiO_2$ (Rege, Padin, and Yang, 1998; Padin and Yang, 2000), and monolayer $AgNO_3$ supported on other substrates (Padin and Yang, 2000). The π-complexation bonds are reasonably understood through molecular orbital studies (Huang, Padin, and Yang, 1999a, 1999b). Among the different sorbents, monolayer $AgNO_3$ appears to be the best. Monolayer spreading of salts on high-surface-area substrates can be accomplished in several ways. One of the methods selected for study is known as *spontaneous monolayer dispersion.* Thermal monolayer dispersion involves mixing a metal salt or oxide with a substrate at a predetermined ratio. This ratio is determined by the amount of salt that is required for monolayer coverage on the surface of the substrate, assuming two-dimensional hexagonal close-packing. The BET surface area of the substrate is first measured. After the finely divided powders of the salt and substrate have been thoroughly mixed, it is heated at a temperature between the Tammann temperature and the melting point of the salt. This method is suitable for laboratory experiments. Another technique is incipient wetness impregnation, which is used in industrial scale for catalyst preparation. It involves preparing a solution of the salt to be dispersed. The solution is then mixed with the substrate, where it is absorbed by the substrate due to incipient wetness. After the substrate has imbibed the solution containing the salt into its pore structure, the sample needs to be heated to remove the solvent. Care needs to be taken when selecting solvents for use in this technique. First, the salt needs to be soluble in the solvent to a sufficient extent to allow enough salt to be dissolved in the volume of solution that can soaked by the pores of the substrate. Second, the solvent selected needs to be able to wet the surface of the substrate. Sorbents prepared by these two methods have been compared carefully (Padin and Yang, 2000). The sorbents prepared by incipient wetness were better. The equilibrium adsorption isotherms for C_2H_4 and C_2H_6 at 70°C on wet impregnated $AgNO_3/SiO_2$ are shown in Fig. 10.

The equilibrium isotherms of C_3H_6 over C_3H_8 at 70°C on $AgNO_3/SiO_2$ prepared by incipient wetness are shown in Fig. 11.

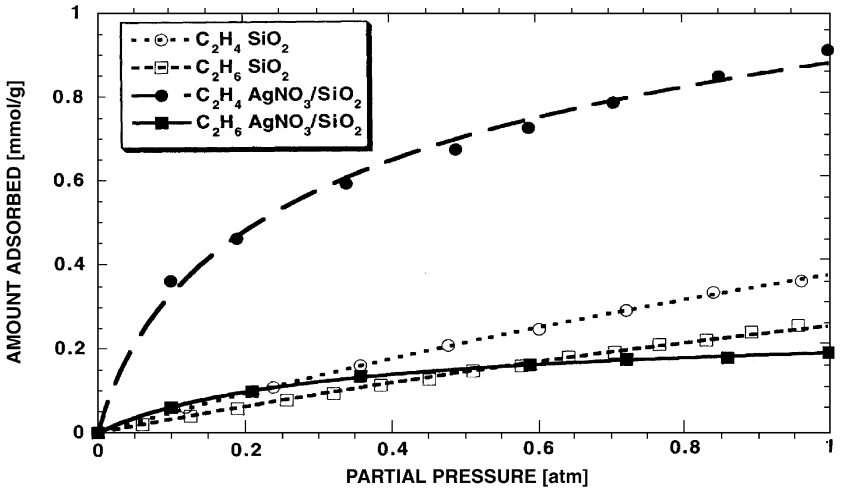

FIG. 10. Equilibrium isotherms of C_2H_4 over C_2H_6 on $AgNO_3/SiO_2$ (by incipient wetness) at 70°C (Padin and Yang, 2000).

From these results, it is seen that the sorbents have excellent selectivities and olefin capacities. The isotherms are also relatively linear. The linearity is desirable for cyclic processes such as PSA (Rege, Padin, and Yang, 1998). Diffusion rates and isotherm reversibilities have also been measured on these systems, and they were all highly suitable for PSA.

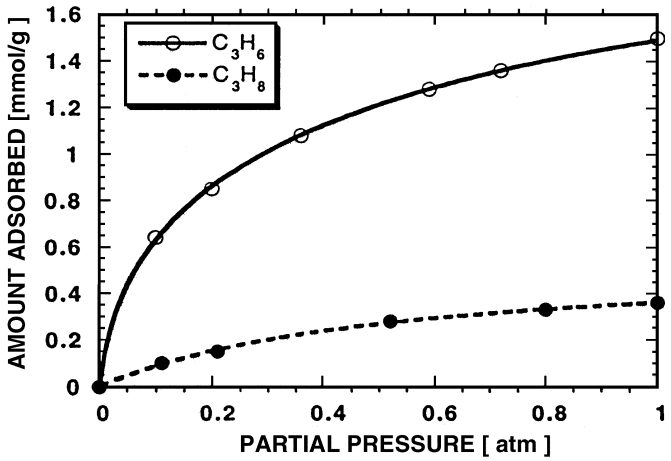

FIG. 11. Equilibrium isotherms of C_3H_6 over C_3H_8 on $AgNO_3/SiO_2$ (by incipient wetness) at 70°C (Padin and Yang, 2000).

B. Effects of Cation, Anion, and Substrate

An experimental as well as theoretical study has been performed in our laboratory on the effects of cations on adsorption (Huang, Padin, and Yang, 1999a). More specifically, a direct comparison of adsorption of CO and ethylene on AgCl and CuCl was made. An *ab initio* molecular orbital study using the effective core potential (ECP) was performed to determine the bond energies and the nature of the bonds between the adsorbates and adsorbents. Experimental results showed that both CO and C_2H_4 adsorbed more strongly on CuCl than on AgCl. However, CO adsorbed much more strongly on CuCl than on AgCl, whereas the difference in heats of adsorption was far less for C_2H_4 on these two sorbents. *Ab initio* molecular orbital calculations correctly predicted the trends. The natural bond orbital (NBO) theory was used to explain the results. The NBO results show that in the two-way π-complexation bonding, the d-π^* back-donation played a major role in determining the bonding for these systems (Huang, Padin, and Yang, 1999a).

The energies of adsorption calculated from molecular orbital theory (Huang, Padin, and Yang, 1999a) are shown in Table IX along with the experimental data. A good comparison between the theoretical values and experimental values is seen. Also, a perfect consistency with the geometry results can be obtained by comparing the differences in the energies of adsorption between the four adsorption systems. It is obvious from the table that CO adsorbed much more strongly on CuCl than on AgCl, with the heat of adsorption being about 7 kcal/mol larger, according to our calculation results. For the adsorption of C_2H_4 on these two adsorbates, however, the difference in the heat of adsorption is only about 4.5 kcal/mol. So it again shows that the difference in the adsorption of CO on CuCl and AgCl is much larger than that of C_2H_4 on these two adsorbates. Experiments and molecular orbital calculations were also performed for C_3H_6 on CuX and AgX (X = halide) (Huang, Padin, and Yang, 1999b).

Despite the fact that Cu^+ is better than Ag^+ in π-complexation, sorbents with Cu^+ are difficult to prepare due to the fact that its simple salts are not

TABLE IX
Energy of Adsorption (in kcal/mol) for MCl–C_2H_4 and MCl-CO Systems (M = Ag or Cu) (Huang, Padin, and Yang, 1999a)

Adsorbate	Adsorbent	Theoretical ΔH	Experimental ΔH (kcal/mol)
C_2H_4	AgCl	11.20	6.9
C_2H_4	CuCl	15.74	8.3
CO	AgCl	9.64	7.5
CO	CuCl	16.56	10.2

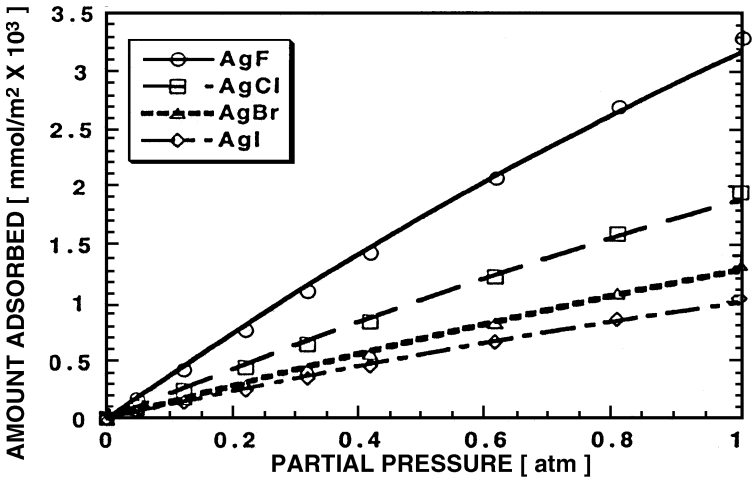

FIG. 12. Normalized C_3H_6 adsorption isotherm on AgX (X=F, Cl, Br, I) salts at 0°C (Huang, Padin, and Yang, 1999b).

water soluble. In addition, Cu^+ is not stable particularly upon exposure to moisture. More work is needed for preparing stable Cu^+ monolayer sorbents.

The effects of both cations and anions on π-complexation have been studied for the adsorption of C_2H_4 and C_3H_6 on CuX and AgX (X=F, Cl, Br, I), by experiment and molecular orbital theory (Huang, Padin, and Yang, 1999b). The following trends of anion and cation effects were obtained for the adsorption of C_2H_4 and C_3H_6 on the metal halides: $F^- > Cl^- > Br^- > I^-$ for anions and $Cu^+ > Ag^+$ for cations. These trends were in excellent agreement with the experimental results. In addition, the theoretical metal–olefin bond energies are in fair agreement with the experimental data. The anion effects are illustrated in Fig. 12.

The effects of substrates on π-complexation were studied by olefin adsorption on monolayer $AgNO_3$ supported on various substrates (Padin and Yang, 2000). The substrates selected were γ-Al_2O_3, SiO_2, and MCM-41. The following trend for olefin adsorption was observed for these substrates:

$$SiO_2 > \text{MCM-41} > \gamma\text{-}Al_2O_3. \tag{20}$$

The silica surface (on both silica gel and MCM-41) provides a better substrate due to the lack of Lewis acid sites (unlike γ-Al_2O_3), and consequently the Ag atoms in these sorbents are more capable of forming π-complexation bonds with olefins. Although the effect of the physical characteristics of a substrate such as surface area and pore size would have on adsorption is clear, the effect of the electronic properties needs to be studied further.

TABLE X
SUMMARY OF THE NBO ANALYSIS OF π-COMPLEXATION BETWEEN MX AND C_2H_4 (HUANG, PADIN, AND YANG, 1999b)

	C → M interaction (σ donation)	M → C interaction (d-π^* back-donation)	Net change
	q_1[a]	q_2[a]	q_1+q_2
CuF–C_2H_4	0.047	–0.089	–0.042
CuCl–C_2H_4	0.052	–0.080	–0.028
CuBr–C_2H_4	0.042	–0.077	–0.035
CuI–C_2H_4	0.030	–0.072	–0.042
AgF–C_2H_4	0.081	–0.073	+0.008
AgCl–C_2H_4	0.058	–0.053	+0.004
AgBr–C_2H_4	0.047	–0.049	–0.002
AgI–C_2H_4	0.032	–0.044	–0.011

[a] q_1 is the amount of electron population increase on valence s orbitals of the metal and q_2 is the total amount of electron population decrease on valence d orbitals of the metal.

C. NATURE OF THE π-COMPLEXATION BOND

The nature of the metal–olefin bond was studied recently in our laboratory by analyzing the natural bond orbital (NBO) results (Huang, Padin, and Yang, 1999b). The main feature of the bonding can be seen from the population changes in the vacant outer-shell s orbital of the metal and those in the d shells of the metal upon adsorption. The NBO analysis, summarized in Tables X and XI, is generally in line with the traditional picture of Dewar (1951), and Chatt and Duncanson (1953) for metal–olefin complexation, i.e., it is dominated by the donation and back-donation contributions, as illustrated by Fig. 13.

An examination of Table XII shows that in all cases the M–C interaction is a dative bond, i.e., donation of electron charges from the π orbital of olefin to the vacant s orbital of metal and, simultaneously, back-donation of electron charges from the d orbitals of M to the π^* orbital of olefin (Fig. 12). This can be interpreted in more detail as follows. When the olefin molecule approaches M^+, some electronic charge is transferred from the C=C π orbital to the valence s orbital of M^+; at the same time, electrons in the filled d orbitals of metal are transferred to the symmetry-matched π^* orbital of olefin. It can be seen from Table XII that upon adsorption, the electron occupancies of the valence s orbitals of Cu and Ag always increase, whereas the total occupancy of their 4d or 5d orbitals always

TABLE XI
SUMMARY OF NBO ANALYSIS OF π-COMPLEXATION BETWEEN MX AND C_3H_6 (HUANG, PADIN, AND YANG, 1999b)

	C → M interaction (σ donation)	M → C interaction (d-π* back-donation)	Net change
	q_1[a]	q_2[a]	q_1+q_2
CuF–C_3H_6	0.046	−0.080	−0.034
CuCl–C_3H_6	0.051	−0.085	−0.034
CuBr–C_3H_6	0.040	−0.071	−0.031
CuI–C_3H_6	0.028	−0.067	−0.039
AgF–C_3H_6	0.081	−0.071	+0.010
AgCl–C_3H_6	0.060	−0.054	+0.006
AgBr–C_3H_6	0.046	−0.047	−0.001
AgI–C_3H_6	0.031	−0.043	−0.012

[a] q_1 is the amount of electron population increase on valence *s* orbitals of the metal, and q_2 is the total amount of electron population decrease on valence *d* orbitals of the metal.

decreases. Obviously this is caused by the donation and back-donation of electrons between metal and olefin, as stated before.

A comparison of the electron population changes in the *s* and *d* orbitals of M before and after adsorption shows that for the CuX–olefin complexes, the overall charge transfer is back-donation. The amount of back-donation is about double the amount of σ-donation. This indicates that the Cu–C bonds contain more metal *d* than metal *s* character and that the strength

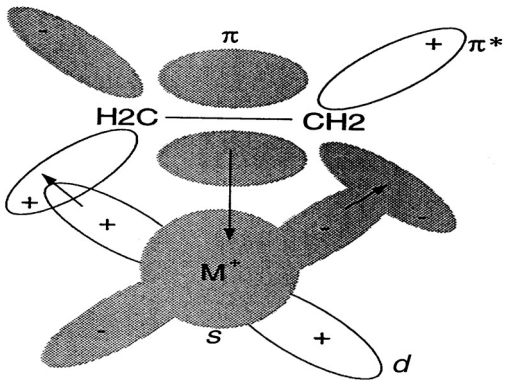

FIG. 13. Schematic representation of a metal–olefin complex showing σ-donation and *d*-π* back-donation.

TABLE XII
ELECTRON POPULATION CHANGES ON *d* ORBITALS OF Cu AND Ag AFTER C_2H_4 ADSORPTION (HUANG, PADIN, AND YANG, 1999b)

	dx_y	d_{xz}	d_{yz}	$d_{x^2-y^2}$	dz^2
$CuF–C_2H_4$	0	0	−0.0823	−0.0015	−0.0051
$CuCl–C_2H_4$	0	0	−0.0604	−0.0012	−0.0187
$CuBr–C_2H_4$	0	0	−0.0558	−0.0011	−0.0197
$CuI–C_2H_4$	0	0	−0.0505	−0.0010	−0.0202
$AgF–C_2H_4$	0	0	−0.0387	0	−0.0342
$AgCl–C_2H_4$	0	0	−0.0370	0	−0.0310
$AgBr–C_2H_4$	0	0	−0.0264	0	−0.0229
$AgI–C_2H_4$	0	0	−0.0239	0	−0.0201

of the covalent bonds depends mainly on the overlap of the metal *d* orbitals with the C hybrid orbitals. For the AgX–olefin complexes, quite differently, the back-donation is almost equal to the σ-donation, which means the σ-donation and back-donation play equally important roles in the bonding of Ag–C. A comparison of the net changes of the electron occupation on the two different metals before and after adsorption shows greater net electron occupation changes on Cu than on Ag upon olefin adsorption. The amount of change indicates the extent of interaction. This is consistent with the conclusion that CuX has a stronger interaction with olefin than AgX.

To gain further insight into the bonding between metal and olefin, Table XII lists the changes in electron populations of the five *d* orbitals of Cu and Ag upon ethylene adsorption.

As we can be seen clearly from the table, the interactions of the five *d* orbitals with ethylene are skewed. Orbitals d_{xy}, d_{xz} and $d_{x^2-y^2}$ have almost no contribution to the overlap with the π^* orbitals of the olefin because there is no or little change in their electron population upon ethylene adsorption. The main depopulation occurs in the d_{yz} and d_{z^2} orbitals. This is because the three inactive orbitals (d_{xy}, d_{xz} and $d_{x^2-y^2}$) are pointing in directions perpendicular to that of d_{yz} (in which plane the three member ring C–C–M lies), so there is little chance for them to overlap with the d_{yz} orbital. The depopulation in the d_{yz} orbital can be explained easily with the classic picture of π-complexation, shown in Fig. 13. However, the smaller amount of population decrease in the d_{z^2} orbitals is not expected. This phenomenon can be understood with the concept of *electron redistribution* that we proposed previously (Chen and Yang, 1996), illustrated in Fig. 14. As shown in Fig. 14, the dumbbell- and doughnut-shaped d_{z^2} orbitals are in the vicinity of the spatial directions of

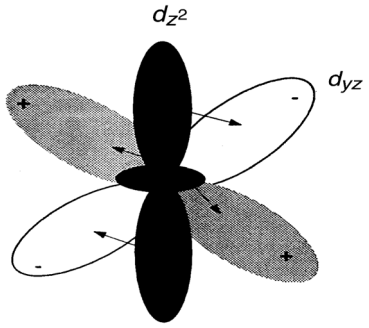

FIG. 14. Schematic representation of electron redistribution from metal d_{z^2} to d_{yz}.

the d_{yz} orbitals, and they can overlap to some extent with the d_{yz} orbitals. This result indicates that there is a considerable electron redistribution between the d_{yz} and d_{z^2} orbitals during the metal–olefin bonding. Obviously, electron redistribution from the d_{z^2} to the d_{yz} orbitals helped enhance the d-π* back-donation.

D. Olefin–Diene Separation and Purification, Aromatic and Aliphatics Separation, and Acetylene Separation

Sorbents and separations based on π-complexation have also found use in other possible applications. Ag^+ ion–exchanged X or Y zeolites showed an excellent capability for purification of olefins by removing trace amounts of corresponding dienes. This has been demonstrated for the butadiene/butene system (Padin, Yang, and Munson, 1999).

For the separations of aromatics from aliphatics, sorbents based on π-complexation have also been studied (Takahashi, Yang, and Yang, 2000). The benzene–cyclohexane pair was used as a model compound. A number of transition metal salts were dispersed in monolayer amounts on a high-surface-area substrate. $PdCl_2$ or $AgNO_3$ dispersed on SiO_2 gel exhibited high equilibrium adsorption ratios of benzene over cyclohexane. $PdCl_2$ loading of 0.88 g/g-SiO_2 showed the best benzene–cyclohexane ratio of 3.2.

For selective acetylene adsorption from other hydrocarbons (e.g., ethylene and ethane), $NiCl_2$ supported on alumina or silica can form reversible π-complexation bonds with acetylene but not olefins. Pure component acetylene–ethylene ratios of up to 3 were obtained (Kodde *et al.,* 2000). The bonding between acetylene and $NiCl_2$ is reasonably understood (Huang and Yang, 1999).

VII. Other Sorbents and Their Unique Adsorption Properties: Carbon Nanotubes, Heteropoly Compounds, and Pillared Clays

A. Carbon Nanotubes

Carbon nanotubes are derivatives of the C_{60} buckyballs. They are formed by graphite (or graphene) sheets rolled up into tubes, generally in the range of 2 to 10 nm in diameter and 200 to 500 nm in length. The multiwall nanotubes were described by Iijima (1991). Single-wall nanotubes were discovered in 1993 (Iijima and Ichihashi, 1993; Bethune *et al.,* 1993). Since their discovery, these materials have attracted intense interests due to their potential in applications in a variety of nanotechnologies (Dresselhaus, Dresselhaus, and Eklund, 1995), such as molecular electronics and scanning probe microscope tips. Of particular interest in adsorption is hydrogen storage.

Much excitement has arisen on recent reports of promising results on carbon nanotubes for hydrogen storage (Dillon *et al.,* 1997; Chambers *et al.,* 1998; Chen, Lin, and Tan, 1999; Liu *et al.,* 1999). High hydrogen adsorption capacities were reported for various carbon nanotubes.Dillon *et al.* (1997) reported that single-wall nanotubes could potentially store up to 5 to 10% by weight of hydrogen at 273 K and 300 torr based on estimates from temperature-programmed desorption data.Chambers *et al.* (1998), using a volumetric system, reported up to 56% by weight of hydrogen storage by multiwall nanotubes at 120 atm and 298 K. More recently, interesting results were reported for using alkali-doped carbon nanotubes for hydrogen storage (Chen, Lin, and Tan, 1999). It was reported that Li- and K-doped carbon nanotubes adsorbed, respectively, 20 wt.% and 14 wt.% of hydrogen at 1 atm and mild temperatures (200 to 400°C for Li-doped and near room temperature for K-doped nanotubes). Lower but still substantial amounts of hydrogen adsorption were also reported for alkali-doped graphite (Chen, Lin, and Tan, 1999). Most recently, Liu *et al.* (1999) reported about 4% by weight of hydrogen adsorption in single-wall nanotubes, at 100 atm and room temperature. It should be noted that the goal for hydrogen storage set by the Department of Energy is 5% by weight for onboard automotive applications.

Needless to say, hydrogen storage with carbon nanotubes has tremendous potentials, yet it is in a highly confusing state. It is difficult, if not impossible, to reproduce data for several reasons. First, carbon nanotubes can be prepared in a number of ways, and it is difficult to reproduce the nanotubes prepared in another laboratory even if the same technique is followed. Second, leakage of hydrogen at high pressures is a notorious problem in the laboratory. In the measurement using a typical volumetric system, the signal for hydrogen adsorption is typically a few psi, which can be easily the amount of leakage.

As mentioned, Chen *et al.* (1999) reported recently in *Science* the most promising results of hydrogen storage in alkali-doped nanotubes at 1 atm pressure. The nanotubes were multiwall nanotubes prepared by catalytic decomposition of methane on $Ni_{0.4}Mg_{0.6}O$. The amount of hydrogen storage was measured with a microbalance. Both the nanotubes and the measurement were easily reproducible. This author has revisited the problem (Yang, 2000). It was found that most of the weight gain was caused by the moisture impurity contained in the hydrogen gas cylinder. Gases supplied in cylinders are frequently contaminated by moisture, and this is particularly the case with hydrogen.

B. Heteropoly Compounds

Heteropoly compounds are a class of crystalline materials with unique structures (Pope, 1983). They can be represented by $H_3XM_{12}O_{40}$. The crystalline structure of the anion $XM_{12}O_{40}$ belongs to the Keggin structure. In this structure, 12 MO_6 octahedra surround a central XO_4 tetrahedron, where M is usually W or Mo and X can be P, As, Si, Ge, B, and others. Although the structures of the heteropoly anions (i.e., the Keggin structure) are well defined and stable (termed primary structure), the structures by which the Keggin units are linked together (termed secondary structure) are less understood. Water is usually the linkage molecule.

$H_3PW_{12}O_{40}$ is one of the most common heteropoly compounds. A distinct X-ray diffraction pattern is seen for $H_3PW_{12}O_{40}.6H_2O$, where the Keggin units are linked by $H^+(H_2O)_2$ bridges, resulting in a body-centered cubic structure and hence the X-ray diffraction pattern. The water molecules can be easily replaced by a number of polar molecules such as alcohols and amines (Misono, 1987).

The unique ability of the heteropoly compound to selectively bind NO was recently found in the author's laboratory (Yang and Chen, 1994; Chen and Yang, 1995). The water linkages in $H_3PW_{12}O_{40}.6H_2O$ can be readily replaced by NO linkages at 50–230°C at low NO concentrations (i.e., under flue-gas conditions) to form $H_3PW_{12}O_{40}.3NO$ (Chen and Yang, 1995). More interestingly, a substantial fraction of the absorbed NO is decomposed into N_2 upon rapid heating of the NO-linked compound (Yang and Chen, 1994; Chen and Yang, 1995). NO is absorbed selectively over other molecules in the flue gas (i.e., CO_2, SO_2, H_2O). These are unique properties of the heteropoly compound. The NO-linked compound has been characterized in detail (Chen and Yang, 1995). This work has been followed by a number of groups, and excellent work has been done by McCormick and coworkers (Herring, McCormick, and Boonrueng, 2000).

C. Pillared Clays

Pillared interlayered clays (PILCs), or pillared clays, are two-dimensional layer materials prepared by exchanging the charge-compensating cations (e.g., Na^+, K^+, and Ca^{2+}) between the swelling phyllosilicate clay layers with large inorganic hydroxy cations, which are polymeric or oligomeric hydroxy metal cations formed by hydrolysis of metal salts. Upon heating, the metal hydroxy cations undergo dehydration and dehydroxylation, forming stable metal oxide clusters that act as pillars, keeping the silicate layers separated and creating interlayer spacing (gallery spaces) of molecualr dimensions. A number of pillared clays can be made easily, such as pillared clays with the following metal oxide pillars: Al, Zr, Cr, Fe, Ti, Si, and Ni.

The cations on the as-made pillared clays are protons. The ion-exchange capacity of the original clay is preserved in the final pillared clay. Hence, PILCs can have very large ion-exchange capacities, for example, 140 meq/g for the Arizona montmorillonite. The high ion-exchange capacities of PILCs are potentially useful for ion exchange applications.

The adsorption propoerties of PILCs and some ion-exchanged PILCs have been studied by a number of groups, including our own. Yang and Baksh (1991) suggested that the pore dimensions in PILCs are not limited by the interlayer spacing (that is determined by X-ray diffraction), but is limited by interpillar spacing. Moreover, the interlayer spacing can be tailored by controlling the number density of pillars that are inserted during the ion-exchange step in the synthesis. The pore-size distributions of the PILCs are actually bimodal: a major portion of pore volume is in pores near 0.6-0.8 nm and a small fraction of pore volume near 0.4 nm (Hutson, Gualdoni, and Yang, 1998; Gil and Grange, 1996; Gandia and Vicente, 2000). By ion exchange with cations of different sizes, the pore dimensions can be furthered tailored (Hutson, Gualdoni, and Yang, 1998). Hence, PILCs offer versatility in both pore-size distribution (by tailoring) as well as surface chemistry (by using different pillars and also by ion exchange). These make PILCs potentially useful as sorbents. However, this promise remains to be fulfilled.

ACKNOWLEDGMENTS

I am grateful to my past and current students and co-workers with whom I have had so much pleasure in learning. Ms. Peggy Kuch's assistance in formatting the manuscript is sincerely acknowledged. This work was supported by the National Science Foundation.

REFERENCES

Adamson, A. W., "Physical Chemistry of Surfaces." 3rd ed., Wiley, New York, 1976.

Alcaniz-Monge, J., de la Casa-Lillo, M. A., Cazorla-Amoros, D., and Linares-Solano, A., *Carbon* **35,** 291 (1997).

Antochsuk, V., and Jaroniec, M., *Chem. Mater.* **12,** 6271 (2000).

Barrer, R. M., "Zeolites and Clay Minerals." Academic Press, New York (1978).

Barrer, R. M., and Gibbons, R. M., *Trans. Faraday Soc.* **61,** 948 (1965).

Barrer, R. M., and Stuart, W. I., *Proc. Roy. Soc.* **A249,** 464 (1959).

Barton, T. J., Bull, L. M., Klemperer, W. G., Loy, D. A., McEnaney, B., Misono, M., Monson, P. A., Pez, G., Sherer, G. W., Vartuli, J. A., and Yaghi, O. M., *Chem. Mater.* **11,** 2633 (1999).

Beck, J. S., Vartuli, J. C., Roth, W. J., Leonowicz, M. E., Kresge, C. T., Schmitt, K. D., Chu, C. T.-W., Olsen, D. H., Sheppard, E. W., McCullen, S. B., Higgins, J. B., and Schlenker, J. L., *J. Am. Chem. Soc.* **114,** 10834 (1992).

Bethune, D. S., Kiang, C. -H., de Vries, M. S., Gorman, G., Savoy, R., Vasquez, J., and Beyers, R., *Nature* **363,** 605 (1993).

Blytas, G. C., Separation of unsaturates by complexing with nonaqueous solutions of cuprous salts, *In* "Separation and Purification Technology" (N. N. Li, and J. M., Clao, Eds.), Chap. 2. Marcel Dekker, New York, 1992.

Breck, D. W., "Zeolite Molecular Sieves," Wiley, New York (1974).

Brinker, C. J., and Sherer, G. W., "Sol-Gel Science." Academic Press, New York, 1990.

Carrasco-Marin, F., Mueden, A., Centeno, T. A., Stoeckli, F., and Moreno-Castilla, C. J., *Chem. Soc. Faraday Trans.* **93,** 2211 (1997).

Chambers, A., Park, C., Baker, R. T. K., and Rodriguez, N. M., *J. Phys. Chem. B* **102,** 4253 (1998).

Chao, C. C., U.S. Patent 4,859,217 (1989).

Chao, C., Sherman, J. D., Mullhaupt, T. J., and Bollinger, C. M., U.S. Patent 5,174,979 (1992).

Chatt, J., and Duncanson, J. A., *J. Chem. Soc.* 2939 (1953).

Chen, P., Wu, X., Lin, J., and Tan, K. L., *Science* **285,** 91 (1999).

Chen, N., and Yang, R. T., *J. Catal.* **157,** 76 (1995).

Chen, N., and Yang, R. T., *Ind. Eng. Chem. Res.* **35,** 4020 (1996).

Cheng, L. S., and Yang, R. T., *Chem. Eng. Sci.* **49,** 2599 (1994).

Cheng, L. S., and Yang, R. T., *Adsorption* **1,** 61 (1995).

Coe, C. G., *in* "Access in Nanoporous Material," (T. J. Pinnavaia and M. F. Thorpe, Eds.), p. 213. Plenum Press, New York, 1995.

Cracknell, R. F., Gubbins, K. E., Maddox, M., and Nicholson, D., *Acc. Chem. Res.* **28,** 281 (1995).

Dewar, M. J. S., *Bull. Soc. Chim., Fr.* **18,** C71 (1951).

Dillon, A. C., Jones, K. M., Bekkedahl, T. A., Kiang, C. -H., Bethune, D. S., and Heben, M. J., *Nature* **386,** 377 (1997).

Doong, S. J., and Yang, R. T., *AIChE Symp. Ser.* **83,** 87, AIChE, New York (1987).

Dresselhaus, M. S., Dresselhaus, G., and Eklund, P. C., "Science of Fullerenes and Nanotubes," Academic Press, New York, 1995.

Eldridge, R. B., *Ind. Eng. Chem. Res.* **32,** 2208 (1993).

Feng, X., Fryxell, G. E., Wang, L. -Q., Kim, A. Y., Liu, J., and Kemmer, K. M., *Science* **276,** 923 (1997).

Ghosh, T. K., Lin, H. D., and Hines, A. L., *Ind. Eng. Chem. Res.* **32,** 2390 (1993).

Gil, A., Gandia, L. M., and Vicente, M. A., *Catal. Rev. Sci. Eng.* **42,** 145 (2000).

Gil, A., and Grange, P., *Colloids and Surfaces* **113,** 39 (1996).

Gilliland, E. R., Bliss, H. L., and Kip, C. E., *J. Am. Chem. Soc.* **63,** 2088 (1941).
Gregg, S. J., and Sing, K. S.W., "Adsorption, Surface Area and Porosity." 2nd ed., Academic Press, New York, 1982.
Hall, C. R., and Holmes, R. J., *Carbon* **31,** 881 (1993).
Henrich, V. E., and Cox, P. A., "The Surface Science of Metal Oxides." Cambridge University Press, Cambridge, UK, 1994.
Herring, A. M., McCormick, R. L., and Boonrueng, S. K., *J. Phys. Chem. B* **19,** 4653 (2000).
Hirai, H., Hara, S., and Komiyama, M., *Angew. Makromol. Chem.* **130,** 207 (1985).
Hirai, H., Kurima, K., Wada, K., and Komiyama, M., *Chem. Lett. (Japan)* **1513** (1985).
Ho, W. S., Doyle., G., Savage, D. W., and Pruett, R. L., *Ind. Eng. Chem. Res.* **27,** 334 (1988).
Horvath, G., and Kawazoe, K., *J. Chem. Eng. Japan* **16,** 470 (1983).
Huang, H. Y., Padin, J., and Yang, R. T., *Ind. Eng. Chem. Res.* **38,** 2720 (1999a).
Huang, H. Y., Padin, J., and Yang, R. T., *J. Phys. Chem. B.* **103,** 3206 (1999b).
Huang, H. Y., and Yang, R. T., *Langmuir* **15,** 7647 (1999).
Huggahalli, M., and Fair, J. R., *Ind. Eng. Chem. Res.* **35,** 2071 (1996).
Humphrey, J. L., and Keller, II, G. E., "Separation Process Technology." McGraw-Hill, New York, 1997.
Huo, Q., Mragolese, D. I., and Stucky, G. D., *Chem. Mater.* **8,** 1147 (1996).
Hutson, N. D., Gualdoni, D. J., and Yang, R. T., *Chem. Mater.* **10,** 3707 (1998).
Hutson, N. D., Rege, S. U., and Yang, R. T., **45,** 724 (1999).
Iijima, S., *Nature* **354,** 56 (1991).
Iijima, S., and Ichihashi, T., *Nature* **363,** 603 (1993).
Iler, R. K., "The Chemistry of Silica." Wiley, New York, 1979.
Israelachilli, J., "Intermolecular and Surface Forces." 2nd ed., Academic Press, New York, 1992.
Izumi, J., "Mitsubishi VOC Recovery Process." Mitsubishi Heavy Industries, Ltd., 1996. Cited from (Tanev and Pinnavaia, 1995).
Jankowska, H., Swiatkowski, A., and Choma, J., "Active Carbon." Ellis Harwood, New York, 1991.
Jaroniec, C. P., Kruk, M., Jaroniec, M., and Sayari, A., *J. Phys. Chem. B.* **102,** 5503 (1998).
Jarvelin, H., and Fair, J. R., *Ind. Eng. Chem. Res.* **32,** 2201 (1993).
Jiang, S., Zollweg, J. A., and Gubbins, K. E., *J. Phys. Chem.* **98,** 5709 (1994).
Jones, R. W., "Fundamental Principles of Sol-Gel Technology." The Institute of Metals, London, 1989.
Kaman, N. K., Anderson, M. T., and Brinker, C. J., *Chem. Mater.* **8,** 1682 (1996).
Kaneko, K., *Carbon* **38,** 287 (2000).
Kaneko, Y., Ohbu, K., Uekawa, N., Fugie, K., and Kaneko, K., *Langmuir* **11,** 708 (1995).
Kaneko, K., Yang, C. M., Ohkubo, T., Kimura, T., Iiyama, T., and Touhara, H., *in* "Adsorption Science and Technology" (D. D. Do, Ed.), p.1. World Scientific Publishers, Singapore, 2000.
Keller, G. E., Marcinkowsky, A. E., Verma, S. K., and Wiliamson, K. D., Olefin recovery and purification via silver complexation, "Separation and Purification Technology" (N. N. Li, and J. M. Calo, Eds.), p.59. Marcel Dekker, New York, 1992.
King, C. J., Separation processes based on reversible chemical complexation, *in* "Handbook of Separation Process Technology" (R. W. Rousseau, Ed.), Chap. 15. Wiley, New York, 1987.
Kodde, A. J., Padin, J., van der Meer, P. J., Mittelmeijer-Hazeleger, M. C., Bliek, A., and Yang, R. T., *Ind. Eng. Chem. Res* **39,** 3108 (2000).
Kulvaranon, S., Findley, M. E., and Liapis, A. I., *Ind. Eng. Chem. Res.* **29,** 106 (1990).
Kumar, R., Kratz, W. C., Guro, D. E., and Golden, T. C., A new process for the production of high purity carbon monoxide and hydrogen, Presented at the Int. Symp. On Separation Technology, Univ. Of Antwerp, Belgium (Aug. 22–27, 1993).
Lamari, M., Aoufi, A., and Malbrunot, P., *AIChE J.* **46,** 632 (2000).

Leon y Leon, C. A., and Radovic, L. R., *in* "Chemistry and Physics of Carbon," (P. A. Thrower, Ed.), Vol. 24, p. 213. Dekker, New York, 1992.
Liu, C., Fan, Y. Y., Liu, M., Cong, H. T., Cheng, H. M., and Dresselhaus, M. S., *Science* **286,** 1127 (1999).
Long, R. B., Separation of unsaturates by complexing with solid copper salts, *in* "Recent Developments in Separation Science" (N. N. Li, Ed.), Vol. 1, p.35. CRC Press, Cleveland, 1972.
Masel, R. I., "Principles of Adsorption and Reaction on Solid Surfaces." Wiley, New York, 1996.
Matranga, K. R., Myers, A. L., and Glandt, E. D., *Chem. Eng. Sci.* **47,** 1569 (1992).
McKee, D. W., U.S. Patent 3,140,933 (1964).
Mellot, C., and Lignieres, J., *in* "Physical Adsorption: Experiment, Theory and Applications" (J. Fraissard, and C. W. Conner. Eds.), Kluwer Academic, Boston, 1997.
Milton, R. M., U.S. Patent 2,882,243, To Union Carbide Corporation, (1959).
Milton, R. M., U.S. Patent 2,882,244, To Union Carbide Corporation, (1959).
Misono, M., *Catal. Rev. Sci. Eng.* **29,** 269 (1987).
Moller, K., and Bein, T., *Chem. Mater.* **10,** 2950 (1998).
Mota, J. P. B., *AIChE J.* **45,** 986 (1999).
Padin, J., and Yang, R. T., *Chem. Eng. Sci.* **55,** 2607 (2000).
Padin, J., Yang, R. T., and Munson, C. L., *Ind. Eng. Chem. Res.* **38,** 3614 (1999).
Pope, M. T., "Heteropoly and Oxopoly Oxometalates," Springer-Verlag, New York, 1983.
Quinn, H. W., Hydrocarbon separations with silver (I) systems, *in* "Progress in Separation and Purification" (Perry, Ed.), Vol. 4, p.133. Interscience, New York, 1971.
Razmus, D. M., and Hall, C. K., *AIChE J.* **37,** 769 (1991).
Rege, S. U., Padin, J., and Yang, R. T., *AIChE J.* **44,** 799 (1998).
Rege, S. U., and Yang, R. T., *AIChE J.* **46,** 734 (2000).
Rigby, M., Smith, E. B., Wakeham, W. A., and Maitland, G. C., "The Forces Between Molecules." Oxford University Press, Fairlaun, NJ 1986.
Rodriguez-Reinoso, F., Molina-Sabio, M., and Munecas, M. A., *J. Phys. Chem.* **96,** 2707 (1992).
Ross, S., and Olivier, J. P., "On Physical Adsorption." Wiley, New York, 1964.
Rouquerol, F., Rouquerol, J., and Sing, K., "Adsorption by Powders and Porous Solids." Academic Press, San Diego, 1999.
Russel, B. P., and LeVan, M. D., *Ind. Eng. Chem. Res.* **36,** 2380 (1997).
Ruthven, D. M., "Principles of Adsorption and Adsorption Processes." Wiley, New York, 1984.
Safarik, D. J., and Eldridge, R. B., *Ind. Eng. Chem. Res.* **37,** 2571 (1998).
Saito, A., and Foley, H. C., *AIChE J.* **37,** 429 (1991).
Salame, I. I., and Bandosz, T. J., *J. Coll. Interf. Sci.* **210,** 367 (1999).
Sayari, A., Liu, P., Kruk, M., and Jaroniec, M., *Chem. Mater.* **9,** 2499 (1997).
Shepelev, Y. F., Anderson, A. A., and Smolin, Y. I., *Zeolites* **10,** 61 (1990).
Steele, W. A., "The Interaction of Gases with Solid Surfaces." Pergamon Press, New York, 1974.
Sun, T., and Ying, J. Y., *Nature* **389,** 704 (1997).
Suzuki, M., *Carbon* **32,** 577 (1994).
Szostak, R., "Molecular Sieves." 2nd ed., Blackie Academic & Professional, New York 1998.
Takahashi, A., Yang, F. H., and Yang, R. T., *Ind. Eng. Chem. Res.* **39,** (2000).
Talu, O., *in* "Fundamentals of Adsorption" (M. Suzuki, Ed.), p. 655. Elsevier, Amsterdam, 1993.
Tanev, P. T., and Pinnavaia, T. J., *Science* **267,** 865 (1995).
Teraoka, Y., Fukunaga, Y., Setaguchi, Y. M., Moriguchi, I., Kagawa, S., Tomonago, N., Yasutake, A., and Isumi, J., *in "Adsorption Science and Technology."* (D. D. Do, Ed.), p. 603. World Scientific Publishers, Singapore, 2000.
Wu, S., Han, S., Cho, S. H., Kim, J. N., and Yang, R. T., *Ind. Eng. Chem. Res.* **36,** 2749 (1999).

Xie, Y. C., and Tang, Y. Q., *Adv. Cat.* **37,** 1 (1990).
Yang, R. T., "Gas Separation by Adsorption Processes." Butterworth, Boston, 1987; Imperial College Press, London, 1997.
Yang, R. T., *Carbon* **38,** 623 (2000).
Yang, R. T., and Baksh, M. S. A., *AIChE J.* **37,** 679 (1991).
Yang, R. T., and Chen, N., *Ind. Eng. Chem. Res.* **33,** 825 (1994).
Yang, R. T., and Hutson, N. D., Lithium-based zeolites containing silver and copper and use thereof for selective adsorption, U.S. Patent 60/114317 (December, 1998).
Yang, R. T., and Kikkinides, E. S., *AIChE Journal,* **41,** 509 (1995).
Yang, F. H., and Yang, R. T., *Carbon,* in press (2001).
Ying, J. Y., Mehnert, C. P., and Wong, M. S., *Angew. Chem. Int. Ed.* **38,** 56 (1999).
Young, D. M., and Crowell, A. D., "Physical Adsorption of Gases." Butterworth, London, 1962.
Zhao, D., Feng, J., Huo, Q., Melosh, N., Frederickson, G. H., Chmelka, B. F., and Stucky, G. D., *Science* **279,** 548 (1998).
Zhao, X. S., Lue, G. Q., and Hu, X., *Chem. Comm.* **1391** (1999).
Zhao, X. S., Lu, G. Q., and Millar, G. J., *Ind. Eng. Chem. Res.* **35,** 2075 (1996).